

Electron quantum optics as quantum signal processing

B. Roussel¹, C. Cabart¹, G. Fève², E. Thibierge¹, P. Degiovanni¹

¹ Univ Lyon, Ens de Lyon, Université Claude Bernard Lyon 1, CNRS, Laboratoire de Physique, F-69342 Lyon, France

² Laboratoire Pierre Aigrain, Ecole Normale Supérieure-PSL Research University, CNRS, Université Pierre et Marie Curie-Sorbonne Universités, Université Paris Diderot-Sorbonne Paris Cité, 24 rue Lhomond, 75231 Paris Cedex 05, France

* Corresponding author: mail: Pascal.Degiovanni@ens-lyon.fr

The recent developments of electron quantum optics in quantum Hall edge channels have given us new ways to probe the behavior of electrons in quantum conductors. It has brought new quantities called electronic coherences under the spotlight. In this paper, we explore the relations between electron quantum optics and signal processing through a global review of the various methods for accessing single- and two-electron coherences in electron quantum optics. We interpret electron quantum optics interference experiments as analog signal processing, converting quantum signals into experimentally observable quantities such as current averages and correlations.

This point of view also gives us a procedure to obtain quantum information quantities from electron quantum optics coherences. We illustrate these ideas by discussing two-mode entanglement in electron quantum optics. We also sketch how signal processing ideas may open new perspectives for representing electronic coherences in quantum conductors and understand the properties of the underlying many-body electronic state.

Copyright line will be provided by the publisher

1 Introduction Electron quantum optics is a new perspective on electronic quantum transport that aims at understanding the behavior of electrons in ballistic quantum conductors using paradigms and methods of quantum optics [1]. This field has emerged from the development of quantum coherent nanoelectronics during the 90s [2,3,4], the demonstration of electronic interferometers [5,6,7] in quantum Hall edge channels and finally the realization of on-demand single-electron sources [8,9].

Importantly, the introduction of single-electron sources has catalyzed a shift from questions about the statistics of charge flowing across a quantum conductor [10,4] to questions about the wavefunctions of elementary excitations carrying the charge. This naturally led to the transposition of photon quantum optics concepts introduced in the 60s by Glauber to coherent quantum nanoelectronics, thus giving birth to the central concepts of electronic coherences [11,12,13,14].

Historically, the scattering theory approach to quantum transport [15,16,17,18,19] had already emphasized the importance of optics concepts in electronic transport. However, electron quantum optics differs from photon

quantum optics because of the Fermi statistics of electrons which changes the nature of the reference “vacuum state” when all sources are switched off. Understanding and extending quantum optics concepts in the presence of such non-trivial vacua was also a motivation for developing electron quantum optics. Even more importantly, electrons are charged particles interacting through Coulomb interactions. As stressed out by M. Büttiker and his collaborators [20,21,22,4], this plays a crucial role in high frequency quantum transport by enforcing charge conservation and gauge invariance [21,4]. Coulomb interactions also raise the basic question of the fate of electronic quasi-particles in a metal, which was the starting point for the Landau-Fermi liquid theory [23].

Electron quantum optics thus offers unprecedented possibilities to study these basic condensed matter physics questions down to the single-electron level. These possibilities are illustrated by recent two-particle interferometry experiments in quantum Hall edge channels which are reviewed in the present volume [24].

Electron quantum optics also establishes a bridge between quantum coherent nanoelectronics and microwave

Copyright line will be provided by the publisher

quantum optics, which now plays an important role in superconducting nanocircuits used for quantum information processing and manipulation [25, 26, 27]. Microwave quantum optics is also crucial for understanding the electromagnetic radiation emitted by a quantum conductor, an important problem rising a growing interest [28, 29, 30, 31, 32, 33, 34].

The purpose of this paper is to reconsider electron quantum optics from a more global perspective by interpreting it in the language of signal processing. In its broadest acceptance, signal processing is an enabling technology that aims at processing, transferring and retrieving information carried in various physical formats called “signals” [35]. Signal processing involves a huge arsenal of techniques to detect, filter, represent, transmit, and finally extract information or recognize patterns within signals. However, the most famous and historically important examples of signals, such as acoustic or electronic signals, are classical. Here, we would like to emphasize that all electron optics experiments realized so far [36, 37, 38, 39] as well as proposals for accessing two-electron coherence [14] can be interpreted in the signal processing language as experiments on signals which are no longer classical: namely electron quantum optics coherences. Electronic interferometers realize analog signal processing operations such as “linear filtering” or “overlaps” on these quantum signals and encode the result into experimentally accessible quantities such as average current and current correlations.

By emphasizing this point of view, we provide a unified view of the recent developments of electron quantum optics and, as we will show by discussing two-particle interferometry, we gain some inspiration towards envisioning new experimental measurement schemes for electronic coherences. Although this has not really been fully exploited yet, it could also suggest new ways of obtaining data by using suitable sources and data processing for optimizing electronic coherence reconstruction [40]. It may also rise interest in the signal processing community towards electron quantum optics and lead to new innovative experimental and theoretical ideas.

In order to develop this point of view, this paper is organized as follows: after briefly recalling the experimental and theoretical context of electron quantum optics in section 2, section 3 reviews the notion of single-electron coherence and the various ways to access this quantity. We will discuss the signal processing operations performed in various single- and two-particle interferometers used to probe single-electron coherence. Our discussion is complementary to that of the review [24] which discusses two-particle interferometry experiments in quantum Hall edge channels and the underlying theory. Here, the same concepts are reviewed with a strong emphasis on the quantum signal processing point of view.

We then turn to two-electron coherence in section 4, and present its definition and its main properties. We in-

troduce its various representations and discuss its non-classical features. We then present its relation to quantum noise of the electrical current, showing the electron quantum optics version of Einstein’s relation between particle number fluctuations and wavefunctions. We show that a whole class of experiments can be interpreted as linear filtering converting the intrinsic second order coherence emitted by a source into current correlations.

In the last section, we will connect electronic coherences to quantum information theoretical quantities. For this purpose, we will explain how to derive effective qubit density matrices from a set of orthogonal single-particle states. In particular, we will illustrate this by discussing electron/hole entanglement in the many-body state generated by a mesoscopic capacitor. We will finally sketch how ideas from signal processing lead to a suitable definition of these density matrices for periodically driven systems.

2 The context of electron quantum optics Let us briefly review the main steps that have led to the development of electron quantum optics.

2.1 Experiments On the experimental side, the integer quantum Hall effect in high mobility 2-dimensional electron gas (2DEG) in AsGa/AsGaAl heterostructures provides the analogous of optical fibers through chiral propagation of charge carriers within the so-called edge channels. Progresses in nanofabrication not only enabled the fabrication of the quantum point contact (QPC), which plays the role of an ideal electronic beam splitter [41, 42, 43], but have also enabled its embedding into complicated geometries such as the electronic Mach-Zehnder interferometer (MZI) [5, 44, 45] and the Samuelsson-Büttiker interferometer [46, 7]. These pioneering experiments showed that, at low temperatures, electronic coherence can be maintained over distances comparable to the size of these circuits (from few to 20 μm) [47]. They have also opened the way to the demonstration and study of more complex electronic circuits in which elements such as QPC, quantum dots and single-electron sources could be placed like optical components on an optical table. As mentioned in the Introduction, the demonstration of the mesoscopic capacitor as an on-demand single-electron source [8] marked the beginning of electron quantum optics. Now, other single-electron sources have been demonstrated in AsGa/AsGaAl, from turnstiles [48, 49], mainly motivated by metrology, to the Leviton source [9] which is reviewed in this volume with great details [50].

Around the same time, progresses in microwave technology and measurement techniques have led to the exploration of high-frequency transport [51, 52], thereby confirming the predictions by Büttiker and his collaborators [53, 21]. From a broader perspective, these developments have opened the way to in-depth experimental investigations of high-frequency quantum coherent nanoelectronics.

2.2 Theory The electron quantum optics formalism was then developed taking advantage of the chirality of electronic transport in quantum Hall systems: in such systems, the optical analogy is exploited at its best by decomposing the quantum conductor, or more generally the electronic circuit, into simple building blocks such as quantum point contacts or energy filters so that an incoming electronic flow is transformed into an outgoing one. Then, within the measurement stage, the average current or the current noise is measured either at zero or at a given high frequency. The resulting formalism bears a close similarity with the input-output formalism of photon quantum optics [54]. In particular, it assumes that electronic coherences are probed within a region where interactions can be neglected. In such a region, electrons propagate freely at a Fermi velocity which will be denoted by v_F throughout the present paper. When electronic coherences are probed at a given position, often corresponding to the position of a detector, they depend on time variables.

Such a description contains an assumption on the screening of Coulomb interactions. For example, we assume that screening at a quantum point contact is good enough to neglect any capacitive coupling between the incoming and outgoing edge channels. As of today, there has been no experimental evidence contradicting this assumption. Within this framework, interaction effects have been studied extensively, starting with MZI. We will very briefly discuss some of these works in section 3.2 mentioning that interaction effects can lead to a breaking of the paradigm of quantum conductors as linear electron quantum optics components. We also refer the reader interested by interaction induced decoherence effects in Hong Ou Mandel (HOM) experiments to [24] as well as [39].

2.3 New systems The rapid development of electron quantum optics has also catalyzed a stream of works whose purpose is to extend its application range to new physical systems.

A first line of research deals with extending electron quantum optics to situations in which interactions potentially lead to a drastic change of the ground state such as in superconductivity. This has led to study of electron quantum optics with Bogoliubov quasi-particles which is reviewed in this volume [55]. Another question is the generalization of electron quantum optics to fractional quantum Hall (FQH) edge channels. Proposals have been made for single quasi-particle and single electron emitted in these systems [56] and the HOM experiment with Lorentzian pulses has been considered [57]. However, a full generalization of electron quantum optics in the FQH regime is still missing, the main problem being the absence of any ideal quasi-particle beam splitter. Nevertheless, perturbative approaches may prove to be useful for experiments whenever the crossover energy scale associated with a constriction [58] is well below the experimentally relevant energy scales.

Another line of research focuses on manipulating the spin degree of freedom at the single-electron level. Quantum spintronics has risen a strong interest in the mesoscopic physics community because of the importance of coherent spin transport and manipulation for quantum information processing. Although the $\nu = 2$ edge channel system had already been envisioned for quantum spintronics [59], 2D topological insulators (TI), such as quantum spin Hall systems [60], are now considered as a potentially important class of systems for electron quantum optics. In these materials, such as CdTe/HgTe and InAs/GaSb quantum wells at zero magnetic field, edge channels are topologically protected from backscattering. They come as counterpropagating pairs with opposite spin polarization (spin-momentum locking). The mesoscopic capacitor built from a 2D TI has been proposed as an on-demand single Kramer pair source emitting two single-electron excitations with opposite spins [61,62]. The HOM experiment has been discussed with such sources [63]. A variant of this source based on a driven antidot has also recently been proposed [64] as well as a different system relying on two quantum dots coupled to a 2D TI via tunneling barriers [65]. Coulomb interactions are expected to play an important role in these systems due to the spatial superposition of two counter-propagating edge channels. Comparing to the $\nu = 2$ quantum Hall edge channel system, interactions among counterpropagating edge systems are expected to induce new effects ranging from resonance effects [66] to fractionalization [67].

Although these developments go beyond the scope of the present paper, it is important to keep in mind that the basic concepts of electron quantum optics can be extended to quantum spintronics in a relatively simple way.

3 Single-electron coherence Let us now review the concept of single-electron coherence and discuss how it can be accessed through single-particle interferometry and two-particle interferometry. Our main message is that, under certain circumstances, the first type of experiments correspond to linear filtering in the signal processing language whereas the HOM experiment performs an analog computation of the overlap of two single-electron coherences.

3.1 Definition and representations Single-electron coherence [11] is defined by analogy with first-order coherence in photon quantum optics [68]:

$$\mathcal{G}_\rho^{(e)}(1|1') = \text{Tr}(\psi(1) \rho \psi^\dagger(1')) \quad (1)$$

where ρ denotes the reduced density operator for the electronic fluid, ψ and ψ^\dagger denote the fermionic destruction and creation field operators and $1 = (\alpha, x, t)$ and $1' = (\alpha', x', t')$ denote edge channel indices and space time coordinates. For spin polarized edge channels, α and α' correspond to spin indices: $\alpha = \alpha'$ then encodes spin populations whereas $\alpha = -\alpha'$ corresponds to spin coherences, thus showing that the formalism of electron quantum optics can be easily extended to account for the spin.

In the following, to simplify notations, channel/spin indices will be dropped out when only one edge channel is involved. single-electron coherence contains all the information on single-electron wavefunctions present in the system. For example, let us consider the N electron state $|\Psi_N\rangle = \prod_{k=1}^N \psi^\dagger[\varphi_k]|\emptyset\rangle$ where the creation operator for an electron in the single-particle state φ_k is defined by:

$$\psi^\dagger[\varphi_k] = v_F \int_{\mathbb{R}} \varphi_k(t) \psi^\dagger(t) dt. \quad (2)$$

This state is obtained by filling mutually orthogonal single-particle states $(\varphi_k)_{k \in \{1, \dots, N\}}$ on top of the electronic vacuum $|\emptyset\rangle$. Then, a straightforward application of Wick's theorem shows that, in the space domain at the initial time:

$$\mathcal{G}_{|\Psi_N\rangle}^{(e)}(x|y) = \sum_{k=1}^N \varphi_k(x) \varphi_k(y)^*. \quad (3)$$

In a metallic conductor, at zero temperature and with all electronic sources switched off, the reference state is a Fermi sea vacuum of given chemical potential $\mu(x)$. Therefore, contrary to the case of photon quantum optics, the single-particle coherence does not vanish when sources are switched off but reduces to the Fermi sea contribution $\mathcal{G}_{F_{\mu(x)}}^{(e)}(t|t') = \langle F_{\mu(x)} | \psi^\dagger(x, t') \psi(x, t) | F_{\mu(x)} \rangle$. On the contrary, the inter-channel single-electron coherence vanishes when all electronic sources are switched off: $\mathcal{G}_F^{(e)}(\alpha, t | \alpha', t') = 0$ for $\alpha \neq \alpha'$.

In electron quantum optics, $\mathcal{G}_\rho^{(e)}$ is considered at a given position x within the electronic circuit, thus leading to a two-time function $\mathcal{G}_{\rho, x}^{(e)}(t|t') = \mathcal{G}_\rho^{(e)}(x, t | x, t')$. When the sources are switched on, the single-electron coherence is different from the Fermi sea contribution and the excess single-electron coherence is defined by subtracting the Fermi sea contribution: $\Delta \mathcal{G}_{\rho, x}^{(e)}(t|t') = \mathcal{G}_{\rho, x}^{(e)}(t|t') - \mathcal{G}_{F_{\mu(x)}}^{(e)}(t|t')$.

The most convenient representation for single-electron coherence is a mixed time-frequency representation called the electronic Wigner distribution function, which captures both temporal evolution and the nature of excitations [40]:

$$W_{\rho, x}^{(e)}(t, \omega) = \int_{-\infty}^{+\infty} v_F \mathcal{G}_{\rho, x}^{(e)}\left(t + \frac{\tau}{2} | t - \frac{\tau}{2}\right) e^{i\omega\tau} d\tau \quad (4)$$

where v_F denotes the Fermi velocity at position x . The electronic Wigner distribution function is real. Its marginal distributions give access to the time-dependent average electric current and to the electronic distribution function $f_e(\omega)$ at position x :

$$f_e(\omega) = \overline{W_{\rho, x}^{(e)}(t, \omega)}^t \quad (5a)$$

$$\langle i(x, t) \rangle_\rho = -e \int_{-\infty}^{+\infty} \Delta W_{\rho, x}^{(e)}(t, \omega) \frac{d\omega}{2\pi} \quad (5b)$$

A classicality criterion for the electronic Wigner distribution function has been formulated [40]: $0 \leq W_{\rho, x}^{(e)}(t, \omega) \leq 1$. When verified, it basically means that $W_{\rho, x}^{(e)}(t, \omega)$ can be interpreted as a time-dependent electronic distribution function. This is the case for a quasi-classically driven Ohmic contact, when $|eV_{ac}| \gg hf$ and $k_B T \gg hf$, f being the driving frequency. In this case, both thermal fluctuations and the ac drive are responsible for multiphoton transitions in the electronic fluid and many electron/hole pairs are generated. On the contrary, for a single-electron excitation, quantum delocalization is responsible for negativities as seen on the example of the MZI [40]. Accessing single-electron coherence would thus enable to discuss the non classicality of the electronic fluid at single-particle level.

3.2 Single-particle interferometry as linear filtering

Introduction In classical signal processing, linear filters transform time-dependent input signals into output signals under the constraint of linearity. Well known examples include linear circuit elements in classical electronics and linear optics elements such as lenses, beam splitters and other various optical devices. These components act as linear filters on the electromagnetic field classical coherence introduced in the 30s [69]. This statement also extends to quantum optics by considering quantum optical coherences introduced by Glauber [68].

In this section, we show that the same statement is true in electron quantum optics provided we use quantum conductors in which interaction effects can be neglected. As an example, we will see how the ideal Mach-Zehnder interferometer [70] or the measurement of the electronic distribution function using a quantum dot as an energy filter [71] realize linear filtering of the excess single-electron coherence $\Delta \mathcal{G}_{\rho, x}^{(e)}(t|t')$, which should therefore be seen as a ‘‘quantum signal’’ depending on two times.

We will then discuss how Coulomb interactions partly – but not totally – invalidate this statement. In particular, we will explain why measuring finite-frequency currents enables to keep track of interaction effects and to recover information on single-electron coherence.

Mach-Zehnder interferometry An ideal electronic Mach-Zehnder interferometer, such as the one depicted on Fig. 1, is characterized by the time of flights $\tau_{1,2}$ along its two arms and the magnetic flux threading it $\Phi_B = \phi_B \times (h/e)$. When an electronic source S is placed on the incoming edge channel 1, the time-dependent outgoing electric current in channel 1 is directly proportional to the excess electronic coherence of the source [70, 40]:

$$\langle i_{1\text{out}}(t) \rangle = \sum_{j=1,2} \mathcal{M}_{j,j} \langle i_S(t - \tau_j) \rangle \quad (6a)$$

$$- 2e |\mathcal{M}_{1,2}| \int_{\mathbb{R}} \cos(\omega\tau_{12} + \phi) \Delta W_S^{(e)}(t - \bar{\tau}, \omega) \frac{d\omega}{2\pi} \quad (6b)$$

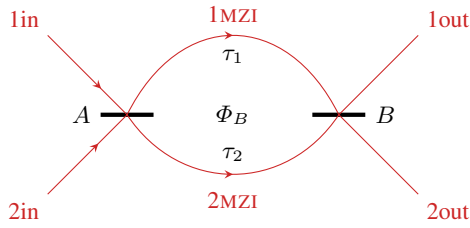


Figure 1 Schematic view of the Mach-Zehnder interferometer: the incoming channels are partitioned at the electronic beam splitter A and then recombined by the beam splitter B . Here τ_1 and τ_2 denote the times of flight across the two branches of the MZI and Φ_B the magnetic flux enclosed by the interferometer.

where $\mathcal{M}_{i,j}$ denotes the product $\mathcal{A}_i \mathcal{A}_j^*$, \mathcal{A}_j being the transmission amplitude of the beam splitters along path j of the interferometer. We have introduced $\tau_{12} = \tau_1 - \tau_2$, $\bar{\tau} = (\tau_1 + \tau_2)/2$ and $\phi = \arg(\mathcal{M}_{1,2} + 2\pi\phi_B)$ which is the phase associated with both beam splitters and the magnetic flux. The first line (Eq. (6a)) does not depend on the magnetic flux and therefore corresponds to classical propagation within each of the two arms of the MZI, whereas the second line (Eq. (6b)) corresponds to quantum interferences between propagations within both arms. Because the average electric current is also proportional to the excess single-electron coherence of the source, the outgoing average current is obtained from the excess incoming coherence $\Delta\mathcal{G}_S^{(e)}$ in channel 1in by a linear filter which we write symbolically $\langle i_{\text{out,dc}} \rangle = \mathcal{L}_{\text{MZI}}[\Delta\mathcal{G}_S^{(e)}]$. Measurements of the Φ_B dependent part of the average dc current for various $\tau_1 - \tau_2$ could then be used to reconstruct single-electron coherence [70].

The key ingredient in this derivation is the absence of electronic interactions. Whenever one replaces the Mach-Zehnder interferometer by an ideal ballistic quantum conductor in which interactions are neglected, the outgoing current in the measurement lead would also be proportional to $\Delta\mathcal{G}_S^{(e)}$. Denoting by $\mathcal{S}(t_f, t_i)$ the scattering amplitude for an electron arriving into the conductor at time t_i and going out towards the measurement lead at time t_f , then the outgoing average time-dependent current is given by

$$\langle i_{\text{out}}(t) \rangle = \int_{\mathbb{R}^2} \mathcal{S}(t, t_+) \mathcal{S}^*(t, t_-) \Delta\mathcal{G}_S^{(e)}(t_+, t_-) dt_+ dt_- \quad (7)$$

which describes a linear filtering of the incoming single-electron coherence $\Delta\mathcal{G}_S^{(e)}$ associated with time-dependent scattering. In particular, this expression is valid within the framework of Floquet scattering theory [72].

On the role of interactions However, as we shall now discuss, because of Coulomb interactions, the situation in electron quantum optics is subtler than in photon quantum optics. It is therefore important to clarify in which

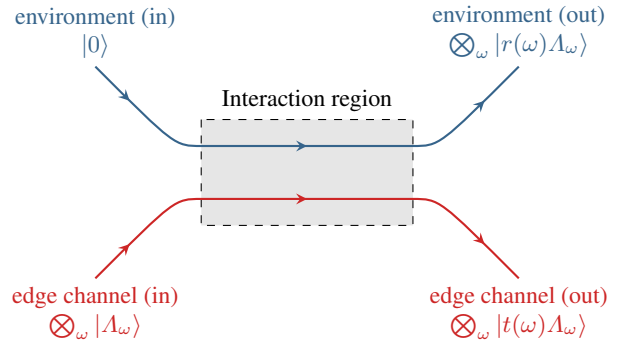


Figure 2 Input/output treatment of a finite-length interaction region (light grey box) in the edge-magnetoplasmon scattering framework: an edge channel (in red) is capacitively coupled to another conductor in the linear response regime, described by an environmental channel (in blue). At zero temperature, the incoming environmental modes are in their vacuum state. When a coherent edge-magnetoplasmon state $|\Lambda\rangle = \otimes_{\omega} |\Lambda_{\omega}\rangle$ is sent in the incoming channel, the outgoing state is $\otimes_{\omega} (|t(\omega)\Lambda_{\omega}\rangle \otimes |r(\omega)\Lambda_{\omega}\rangle)$ where $t(\omega)$ denotes the edge-magnetoplasmon transmission amplitudes across the interaction region and $r(\omega)$ the amplitude to be scattered into environmental modes.

situations the linear filtering paradigm is valid and when it is not valid.

To begin with, let us consider a simple situation in which the source is placed at the input of a finite-length interaction region, as depicted on Fig. 2. For simplicity, we assume that this interaction region can be described within the edge-magnetoplasmon scattering formalism [73,74]: the incoming edge-magnetoplasmon mode at a given frequency is scattered elastically between the corresponding outgoing mode and environmental modes associated with other electrical degrees of freedom present in the problem. The environment can involve edge channels or any neighboring linear circuit modeled as a transmission line with a frequency-dependent impedance [75]. Such a modelization is valid as long as all the components of the system are in the linear response regime. This formalism was used to compute the effect of Coulomb interactions on coherent current pulses [76] and single-electron excitations [74, 77]. Equivalently, because they induce inelastic processes, Coulomb interactions turn a quantum conductor into a non-linear component from the electron quantum optics point of view. Consequently, in general, the excess outgoing single electron coherence is not a linear filtering of the incoming one!

A criterion for the validity of the electronic scattering theory approach to quantum transport at finite frequencies is that the frequency dependence of the electronic scattering matrix of a quantum conductor can be neglected [4]. Single- to few-electron excitations emitted by

electron quantum optics sources such as the mesoscopic capacitor [8] or the Leviton source [9] as well as periodic electric currents generated using an advanced waveform generator usually define a frequency scale in the range of one to few tens of GHz. On the other hand, an extended conductor such as a MZI has a scattering matrix varying over frequency scales of the order of the inverse of the time of flight of the conductor. For a 10 μm interferometer, it is of the order of 10 GHz. This is why extended quantum conductors such as MZIs fail to satisfy this criterion. The important stream of theoretical work on interaction-induced decoherence [78,79,80,81,82] in MZI interferometers illustrate the full complexity of understanding interaction effects in such extended quantum conductors. More recent works [83,84] dealing with the propagation of individualized energy-resolved single-electron excitations in a MZI are directly relevant for electron quantum optics but also show that this problem is not yet fully understood even at the single-electron level.

By contrast, Coulomb interaction effects can be neglected over a much broader frequency range in the QPC which is an almost point-like electronic beam-splitter. As we shall see in the next section, this plays a very important role for the HOM and HBT experiments.

Last but not least, the average finite-frequency currents are relatively robust to the effect of Coulomb interactions: whenever all electrical components respond linearly to the incoming excitation, the edge-magnetoplasmon scattering matrix can be used to reconstruct the incoming average finite frequency currents from the outgoing ones. Measurements of finite-frequency average currents have been successfully developed in the 1-11 GHz range to perform the first direct measurement of edge-magnetoplasmon scattering amplitudes [85].

3.3 Two-particle interferometry as overlap

Motivation Although amplitude interferometry relies on the measurement of average currents, it does not seem well suited to perform single-electron tomography. First of all, as in optics, it would require a perfect control on electronic optical paths down to the Fermi wavelength. More importantly, as discussed in the previous section, Coulomb interactions prevent reconstructing the incoming single-electron coherence from the experimental signals.

This situation is very similar to what happened in astronomy in the 30s and 40s: attempts at directly measuring the diameter of normal stars using amplitude interferometry were plagued by atmospheric turbulences and by the technological challenge of building a large optical interferometer. However, a way to circumvent this bottleneck was found by Hanbury Brown and Twiss (HBT) in the 50s [86]: their idea was to measure intensity correlations [87] since these contain interferences between waves emitted by pairs of atoms on the star. In quantum optics, the HBT effect ultimately relies on two-photon interferences [88]. In the 80s, the Hong Ou Mandel (HOM) experiment [89] also demonstrated two-particle interferences for identical par-

ticles (photons). Since then, two-particle interference effects have been observed in many different contexts, from stellar interferometry to nuclear and particle physics [90] and more recently with bosonic as well as fermionic cold atoms [91]. Recent experiments demonstrate a higher degree of control by using independent single-photon [92] and single atom sources [93].

In this section, we review how the HOM experiment can be used to measure the overlap of the excess single-particle coherences arriving at a beam splitter. Remarkably, this result is true not only for electrons but for any fermionic or bosonic excitation. In photon quantum optics, it forms the basis of homodyne tomography [94,95] recently used to characterize few-photon states in the optical domain [96]. In the microwave domain, the HOM scheme has been used to access photon quantum optical correlations from electrical measurements [27,26] and forms the basis of a tomography scheme for itinerant microwave photons [97,25].

Theoretical analysis In electron quantum optics, the HBT and HOM experiments are demonstrated by sending electronic excitations generated by one or two electronic sources on an ideal electronic beam splitter, as depicted on Fig. 3.

In order to make a precise analogy with photon quantum optics, keeping in mind that in electron quantum optics, the vacuum is the reference Fermi sea and not a true vacuum, we consider that the electronic analogue of the table-top HBT experiment (Fig. 3a) [87] is realized when one of the incoming channels is fed with the reference Fermi sea (S_1 or S_2 being off). By the same analogy, the electronic HOM experiment (Fig. 3b) corresponds to situations with both electronic sources in the incoming channels switched on. Finally, whereas in photon quantum optics, the arrival of individual photons can be recorded, in electronics, the quantities of interest are the current correlations at zero frequency in the two outgoing branches.

Let us focus on the outgoing current noise in channel 1. A first important point is that the low-frequency current noise does not depend on the distance to the QPC: interaction effects lead to edge-magnetoplasmon scattering among the various outgoing edge channels close to the one considered but the total power remains the same. This is why HBT/HOM interferometry is immune to interaction effects in the measurement stage (beyond the QPC). In the same way, the intensity correlations measured in an optical stellar HBT interferometer are not blurred by atmospheric turbulences.

Consequently, what we need is the excess low frequency current noise just after the QPC when both sources S_1 and S_2 are switched on. It is the sum of three contributions [40]:

$$\Delta S_{11}^{(S_1 \& S_2)} = \Delta S_{11}^{(S_1)} + \Delta S_{11}^{(S_2)} + \Delta S_{11}^{(\text{HOM})} \quad (8)$$

where $\Delta S_{11}^{(S_1)}$ and $\Delta S_{11}^{(S_2)}$ are the excess current noise when only the source S_1 (resp. S_2) is switched on. These

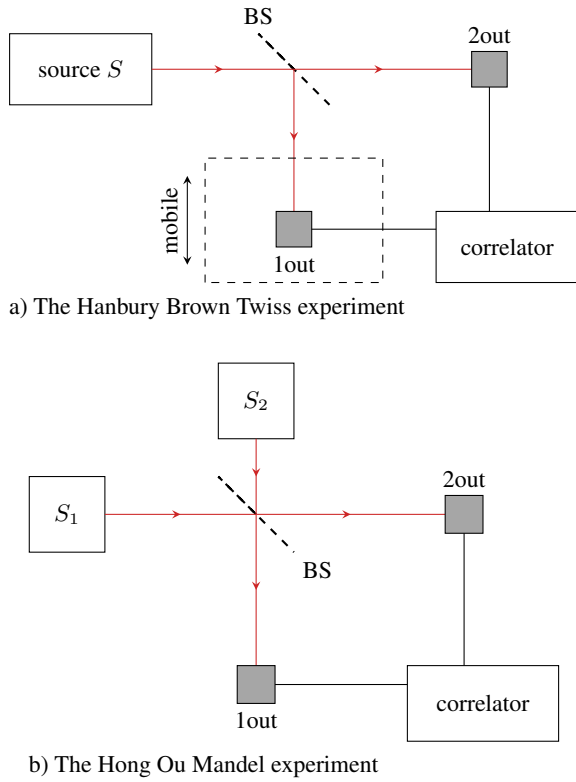


Figure 3 Principle of the HBT and HOM experiments: in the optical HBT experiment (a), excitations emitted by a single source S are partitioned at the beamsplitter BS whereas in the HOM experiment (b), excitations emitted by two sources S_1 and S_2 are sent onto BS. In optics, one performs a time-resolved detection of photons. In the electronic case, the beamsplitter is a QPC, and one measures current correlations between 1out and 2out or current noise in the 1out channel. In the case of the HBT experiment, vacuum is replaced by the reference Fermi sea.

contributions correspond to the excess noise in HBT experiments performed on each of the sources. The last term

$$\Delta S_{11}^{(\text{HOM})} = -2e^2 RT \int_{\mathbb{R}^2} \Delta W_{1\text{in}}^{(e)}(t, \omega) \Delta W_{2\text{in}}^{(e)}(t, \omega) \frac{dt d\omega}{2\pi} \quad (9)$$

is the overlap of the excess single-electron coherences arriving at the QPC [40] (R and T denoting the reflection and transmission probabilities of the QPC). Eq. (9) encodes the effect of two-particle interferences between the excitations emitted by these sources. Note that the time delay of the two sources can be controlled and therefore a single experimental run gives access to the time-shifted overlaps of the excess electronic Wigner functions of the two sources. Finally, the minus sign comes from the fermionic statistics of electrons.

The two first terms also involve two-particle quantum interferences. Because they contain information on coherences of each of the sources, they will be discussed in section 4. Our point here is to emphasize that the electronic HOM experiment automatically encodes into the experimental signal what the signal processing community would call the sliding inner product of the quantum signals formed by the incoming excess single-electron coherences in channels 1 and 2. This is why the HOM experiment is so important: it can be used to test for unknown excess electronic Wigner functions by looking at their overlaps with themselves or with the ones generated by controlled and calibrated sources. This idea has been expanded to describe a generic tomography protocol for reconstructing an unknown excess single-electron coherence from its overlaps with coherences generated by suitable ac + dc drives [98]. We refer the reader to [24] in the same volume for a detailed description of this protocol.

Experimental demonstration The electronic HBT experiment has been demonstrated in the late 90s using dc sources [3,2] and more recently using single-electron sources [99] which were then used to perform the electronic HOM experiment [36]. These experiments have paved the way to measurements and studies of electron decoherence down to the single-electron level through HOM interferometry.

The idea of the tomography protocol has been recently demonstrated by D.C. Glatli's group [37]: in this experiment, a stream of Lorentzian pulses is sent onto a beam splitter whose other incoming channel is fed with a small ac drive on top of a dc bias. Measurement of the low-frequency noise then enables reconstructing the photo-assisted transition amplitudes which, in this case, contain all the information on single-electron and higher-order electronic coherences [9]. This experiment being performed in a 2DEG at zero magnetic field, interaction effects can be neglected and the experiment leads to the reconstruction of the Leviton single-electron coherence [37].

As reviewed in this volume [24], the HOM experiment has also recently been used to probe interaction effects within quantum Hall edge channels. In these experiments, performed at filling factor $\nu = 2$, two single-electron sources are located at some distance of the QPC and interaction effects are strong enough to lead to quasi-particle destruction, as suggested by energy relaxation experiments [100]. First, the HOM effect was used to probe how interactions lead to fractionalization of classical current pulses [38] in qualitative agreement with the neutral/charge edge-magnetoplasmon mode model [80] which had been already probed through energy relaxation experiments [101] and high-frequency admittance measurements [85]. But the real strength of HOM experiment comes from its ability to probe electronic coherence in a time- and energy-resolved way. It was thus recently used to study quantitatively the effect of Coulomb interactions on energy-resolved single-electron excitations (called Landau

excitations) [39]. The experimental data confirm theoretical predictions and validate the decoherence scenario based on edge-magnetoplasmon scattering [102, 77].

4 Two-electron coherence Let us now turn to two-electron coherence. After briefly reviewing its definition and properties, introducing the two-electron Wigner distribution function will enable us to emphasize its non-classical features arising from Fermi statistics. We will then turn to two-particle interferometry and show that, under appropriate hypotheses, these experiments perform a linear filtering on the intrinsic two-electron coherence, thus generalizing what was discussed in section 3.2.

4.1 Definition and representations

Definition Two-electron coherence is defined by direct analogy with Glauber's second-order photonic coherence [13]:

$$\mathcal{G}_\rho^{(2e)}(1, 2|1'2') = \text{Tr}(\psi(2)\psi(1)\rho\psi^\dagger(1')\psi^\dagger(2')) \quad (10)$$

where $1 = (\alpha_1, x_1, t_1)$ and $2 = (\alpha_2, x_2, t_2)$, $\alpha_{1,2}$ being channel indices, and similarly for $1'$ and $2'$. Its physical meaning can be obtained by computing the two-electron coherence for the state $|\Psi_N\rangle$ defined in section 3.1. The result is a sum over all the two-electron wavefunctions $\varphi_{k,l}(x, y) = \varphi_k(x)\varphi_l(y) - \varphi_k(y)\varphi_l(x)$ ($k < l$) that can be extracted from the N single-particle wavefunctions $(\varphi_k)_{k \in \{1, \dots, N\}}$ [14]:

$$\mathcal{G}_{|\Psi_N\rangle}^{(2e)}(x_1, x_2|x'_1, x'_2) = \sum_{k < l} \varphi_{k,l}(x_1, x_2) \varphi_{k,l}(x'_1, x'_2). \quad (11)$$

Two-electron coherence at a given position is a function of four times $(t_1, t_2; t'_1, t'_2)$.

Fermionic statistics and two-electron coherence

Although its definition and Eq. (11) may suggest that two-electron coherence bears similarity with single-electron coherence discussed in the previous section, it already contains all the counter-intuitive aspects of quantum indiscernability. Electrons being fermions, the two-electron coherence satisfies the following antisymmetry properties:

$$\mathcal{G}_\rho^{(2e)}(1, 2|1'2') = -\mathcal{G}_\rho^{(2e)}(2, 1|1'2') \quad (12a)$$

$$= -\mathcal{G}_\rho^{(2e)}(1, 2|2'1') \quad (12b)$$

Antisymmetry leads to the global symmetry of two-electron coherence $\mathcal{G}_\rho^{(2e)}(1, 2|1'2') = \mathcal{G}_\rho^{(2e)}(2, 1|2'1')$ expressing that the order of detection of electrons does not matter. It also implies that two-electron coherence vanishes whenever $1 = 2$ or $1' = 2'$: this is the Pauli exclusion principle. Together with the conjugation relation

$$\mathcal{G}_\rho^{(2e)}(1, 2|1'2')^* = \mathcal{G}_\rho^{(2e)}(1', 2'|1, 2), \quad (13)$$

antisymmetry implies that two-electron coherence is defined by its values for only 1/8-th of the possible arguments.

The intrinsic two-electron coherence emitted by a source can be defined from the second-order electronic coherence by subtracting not only the Fermi sea contribution but also all processes contributing to two-electron detection and involving the excess single-electron coherence of the source. These involve classical contributions as well as quantum exchange contributions [14]:

$$\mathcal{G}_\rho^{(2e)}(1, 2|1', 2') = \mathcal{G}_F^{(2e)}(1, 2|1', 2') \quad (14a)$$

$$+ \mathcal{G}_F^{(e)}(1|1') \Delta \mathcal{G}_\rho^{(e)}(2|2') + \mathcal{G}_F^{(e)}(2|2') \Delta \mathcal{G}_\rho^{(e)}(1|1') \quad (14b)$$

$$- \mathcal{G}_F^{(e)}(1|2') \Delta \mathcal{G}_\rho^{(e)}(2|1') - \mathcal{G}_F^{(e)}(2|1') \Delta \mathcal{G}_\rho^{(e)}(1|2') \quad (14c)$$

$$+ \Delta \mathcal{G}_\rho^{(2e)}(1, 2|1', 2'). \quad (14d)$$

Eq. (14) should be seen as a definition of the intrinsic two-electron coherence $\Delta \mathcal{G}_\rho^{(2e)}$ from the total two-electron coherence, the Fermi sea two-electron coherence and lower-order electronic coherences. The second term (14b) is present for classical particles and represent classical correlations in which the origin of the two detected particles can be traced back either to the Fermi sea or the source. Such back-tracking is not possible for the exchange terms (14c) whose minus sign comes from the fermionic statistics. Note that Eq. (14) is fully compatible with Eq. (11). Moreover, for a state obtained by adding a single-electron or hole excitation to the Fermi sea, the intrinsic two-electron coherence vanishes as expected for a source emitting only one excitation.

The frequency domain representation of two-electron coherence Exactly as in the case of single-electron coherence, the nature of excitations can be obtained by going to the frequency domain:

$$\begin{aligned} \tilde{\mathcal{G}}_\rho^{(2e)}(\omega_+|\omega_-) &= \int_{\mathbb{R}^4} \mathcal{G}_\rho^{(2e)}(\mathbf{t}_+|\mathbf{t}_-) e^{i(\omega_+ \cdot \mathbf{t}_+ - \omega_- \cdot \mathbf{t}_-)} d^2 \mathbf{t}_+ d^2 \mathbf{t}_- \end{aligned} \quad (15)$$

where $\mathbf{t}_+ = (t_1, t_2)$ and $\mathbf{t}_- = (t'_1, t'_2)$ are respectively conjugated to $\omega_+ = (\omega_1, \omega_2)$ and $\omega_- = (\omega'_1, \omega'_2)$. Note that antisymmetry properties (12) are also true in the frequency domain.

The diagonal of the frequency domain ($\omega_- = \omega_+ = (\omega_1, \omega_2)$) can be divided into quadrants depicted on Fig. 4 that describe the elementary two-particle excitations. When ω_1 and ω_2 are both positive, we have an electronic pair whereas when they are both negative, we have a pair of holes. In the case one is positive and the other negative, we have an electron hole pair. Note that this classification is compatible with the permutation $\omega_1 \leftrightarrow \omega_2$.

The full frequency domain (ω_+, ω_-) can then be decomposed into 4D simplexes based on these quadrants for the diagonal. This will naturally be compatible with the antisymmetry properties of the two-electron coherence. Di-

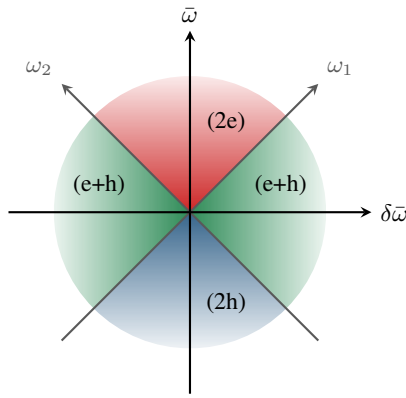


Figure 4 Nature of two-particle excitations: partitioning the diagonal plane $(\omega_1, \omega_2) = (\bar{\omega} + \delta\bar{\omega}/2, \bar{\omega} - \delta\bar{\omega}/2)$ in two sectors associated with pairs of electrons (2e) and pairs of holes (2h) and two sectors associated with electron/hole pairs (e+h).

agonal simplexes are based on ω_+ and ω_- that both describe the same type of excitation. This leads to a two-electron simplex, a two-hole simplex and two electron/hole pair simplexes respectively containing the contributions of two-electron, two-hole and electron/hole pair excitations. The off-diagonal simplexes where ω_+ and ω_- do not belong to the same quadrant describe coherences between these four different two-particle excitations.

4.2 The Wigner representation of two-electron coherence

Definition The Wigner representation of two-electron coherence is defined in the same way as for single-electron coherence, that is as a Fourier transform with respect to the time differences $\tau_j = t_j - t'_j$. When considering a diagonal two-electron coherence in the channel indices ($\alpha_j = \alpha'_j$ for all $j = 1, 2$), this leads to a real function

$$W_{\rho,x}^{(2e)}(t_1, \omega_1; t_2, \omega_2) = \int_{\mathbb{R}^2} v_F^2 \mathcal{G}_{\rho,x}^{(2e)} \left(\mathbf{t} + \frac{\boldsymbol{\tau}}{2} \middle| \mathbf{t} - \frac{\boldsymbol{\tau}}{2} \right) e^{i\boldsymbol{\omega} \cdot \boldsymbol{\tau}} d^2\boldsymbol{\tau}. \quad (16)$$

The Wigner representation of the excess two-electron coherence $\Delta W_{\rho,x}^{(2e)}(t_1, \omega_1; t_2, \omega_2)$ is defined by Eq. (16) from the excess two-electron coherence. Whenever Wick's theorem applies, the total two-electron coherence can be computed in terms of the single-electron one:

$$\mathcal{G}_{\rho,x}^{(2e)}(1, 2|1', 2') = \mathcal{G}_{\rho,x}^{(e)}(1|1') \mathcal{G}_{\rho,x}^{(e)}(2|2') - \mathcal{G}_{\rho,x}^{(e)}(1|2') \mathcal{G}_{\rho,x}^{(e)}(2|1'). \quad (17)$$

and, using Eqs. (14), the same equation also describes the intrinsic two-electron coherence in terms of the excess single-electron coherence. The first term contributes to the two-electron Wigner distribution through the prod-

uct $W_{\rho,x}^{(e)}(t_1, \omega_1) W_{\rho,x}^{(e)}(t_2, \omega_2)$ which corresponds to independent classical particles. The second term comes from quantum exchange and, as we shall see now, is responsible for non-classical features of the two-electron Wigner distribution function.

Non classicality of two-electron coherences In the case of single-electron coherence, a definition of classicality was given [40] based on the idea of interpreting $W_{\rho,x}^{(e)}(t, \omega)$ as a time-dependent electronic distribution function compatible with the Pauli exclusion principle. It is natural to extend this definition to the two-particle case: $W_{\rho,x}^{(2e)}(t_1, \omega_1; t_2, \omega_2)$ would be called classical if it takes values between 0 and 1. Of course, if we consider the inter-channel two-electron Wigner distribution associated with the inter-channel two-electron coherence $\mathcal{G}_{\rho,x}^{(2e)}(1, t_1; 2, t_2|1, t'_1; 2, t'_2)$, then when the two channels are not correlated, we have $W_{\rho,x}^{(2e)}(1, t_1, \omega_1; 2, t_2, \omega_2) = W_1^{(e)}(t_1, \omega_1) W_2^{(e)}(t_2, \omega_2)$ as expected for uncorrelated classical objects¹. Consequently, if the two-electronic Wigner distribution in channels 1 and 2 are classical, the inter-channel two-electron Wigner distribution is also classical. But as we shall see now, because of its antisymmetry properties, the two-electron Wigner distribution in a single channel exhibits non classical features.

To illustrate this point, let us consider mutually orthogonal time-shifted wave-packets: $\varphi_1(t) = \varphi_e(t - \tau/2)$ and $\varphi_2(t) = \varphi_e(t + \tau/2)$. The intrinsic two-electron Wigner distribution function associated with the state $|\Psi_2\rangle = \psi^\dagger[\varphi_1]\psi^\dagger[\varphi_2]|F\rangle$ is then

$$\begin{aligned} \Delta W_{|\Psi_2\rangle}^{(2e)}(t_1, \omega_1; t_2, \omega_2) = & W_{\varphi_1}(t_1, \omega_1) W_{\varphi_2}(t_2, \omega_2) \\ & + W_{\varphi_2}(t_1, \omega_1) W_{\varphi_1}(t_2, \omega_2) \\ & - 2 \cos((\omega_1 - \omega_2)\tau) W_{\varphi_e}(t_1, \omega_1) W_{\varphi_e}(t_2, \omega_2). \quad (18) \end{aligned}$$

When considering a quasi-classical electronic wavepacket, such that $W_{\varphi_e}(t, \omega)$ is almost everywhere positive, we see that the last term contains interference fringes due to the $\cos((\omega_1 - \omega_2)\tau)$ factor. When φ_1 and φ_2 are well separated, negativities appear which reflect the non-classical nature of two-electron wavefunctions within a single edge channel. Note that the dependence in $\omega_1 - \omega_2$ comes from the fact that, in the above example, φ_1 and φ_2 are time-shifted wavepackets. Energy-shifted wavepackets would lead to oscillations in $t_1 - t_2$ analogous to Friedel oscillations in solid-state physics. In full generality, the quantum exchange interference terms present both a time and an energy dependence and this prevents $W^{(2e)}$ to be interpreted as a time-dependent two-electron distribution function.

Similarly, the two-electron Wigner distribution function of the equilibrium state at electronic temperature T_e

¹ Here the channel index breaks the indiscernability between electrons within the two different channels.

and vanishing chemical potential is given by

$$W_{\mu=0, T_e}^{(2e)}(t_1, \omega_1; t_2, \omega_2) = f_{T_e}(\omega_1) f_{T_e}(\omega_2) \quad (19a)$$

$$-4\pi k_B T_e \delta(\omega_1 - \omega_2) f_{B, T_e}(\omega_{\text{tot}}) \frac{\sin(\omega_{\text{tot}} t_{12})}{\sinh(t_{12}/\tau(T_e))} \quad (19b)$$

where $\omega_{\text{tot}} = \omega_1 + \omega_2$, $t_{12} = t_1 - t_2$ and $\tau(T) = \hbar/k_B T$ denotes the thermal coherence time. Here f_{T_e} is the Fermi-Dirac distribution at temperature T_e and $\mu = 0$ whereas $f_{B, T}(\omega) = 1/(e^{\hbar\omega/k_B T} - 1)$ denotes the Bose-Einstein distribution at temperature T . The singular second term (19b) expresses the Pauli exclusion principle and presents strong oscillations in t_{12} . Therefore $W_{\mu=0, T_e}^{(2e)}$ cannot be interpreted as a time-dependent electronic distribution.

4.3 Relation to current noise Let us now describe the precise relation between two-electron coherence and the excess current noise $\Delta S_i(t, t')$ defined as the excess of

$$S_i(t, t') = \langle i(t') i(t) \rangle - \langle i(t) \rangle \langle i(t') \rangle. \quad (20)$$

Since sub-nanosecond time-resolved measurements are not available in electronics, $S_i(t, t')$ is not directly accessible. However, finite-frequency current noise measurements [103] give access to the noise spectrum which is a time-averaged quantity. More recently, partial measurements of the time-dependent current noise power spectrum have been performed. This quantity is defined as the Wigner function associated with excess current correlations:

$$W_{\Delta S_i}(t, \omega) = \int_{\mathbb{R}} \Delta S_i \left(t - \frac{\tau}{2} \middle| t + \frac{\tau}{2} \right) e^{i\omega\tau} d\tau. \quad (21)$$

This is achieved through a recently developed homodyne measurement technique [104] which has been used to probe the squeezing of the radiation emitted by a tunnel junction. The canonical anticommutation relations and definition (14) imply that the quantity defined by Eq. (21) is directly related to the intrinsic two-electron coherence by

$$W_{\Delta S_i}(t, \omega) + W_{\langle i \rangle}(t, \omega) = -e \langle i(t) \rangle \quad (22a)$$

$$-e^2 \int_{\mathbb{R}} h_{\mu}(\omega, \omega') \Delta W_{\rho}^{(e)}(t, \omega') \frac{d\omega'}{2\pi} \quad (22b)$$

$$+ e^2 \int_{\mathbb{R}} v_F^2 \Delta \mathcal{G}_{\rho}^{(2e)} \left(t + \frac{\tau}{2}, t - \frac{\tau}{2} \middle| t + \frac{\tau}{2}, t - \frac{\tau}{2} \right) e^{i\omega\tau} d\tau \quad (22c)$$

where $h_{\mu}(\omega, \omega') = f_{\mu}(\omega - \omega') + f_{\mu}(\omega + \omega')$ and $W_{\langle i \rangle}(t, \omega)$ denotes the Wigner-Ville transform [105] of the average time-dependent current. The first term (22a) is a Poissonian contribution associated with the granular nature of charge carriers. The second term (22b) arises from two-particle interferences between excitations generated by the source

and electrons within the Fermi sea. These contributions are called the HBT contributions since these two-particle interferences are precisely what is measured in an HBT experiment. Finally, the last term (22c) corresponds to the intrinsic two-electron coherence contribution to the current noise. This equation is indeed the electron quantum optics version of the famous relation on fluctuations of particle number in an ideal Bose gas [106] where the term (22c) minus $W_{\langle i \rangle}(t, \omega)$ corresponds to Einstein's quadratic term. Finally, the non triviality of the Fermi sea vacuum is responsible for the term (22b).

This equation also relates electronic coherences to the quantum optical properties of the edge magnetoplasmons within the edge channel and therefore of the photons radiated into a transmission line capacitively coupled to the edge channel as in [74]. It therefore establishes a bridge between electron quantum optics and the recently studied quantum optics of noise [29].

Finally, let us stress that Eq. (22), which is also valid in the presence of interactions, shows that accessing single-electron coherence as well as the current noise gives access to the diagonal part of two-electron coherence, as expected since the latter contains all the information on time resolved two-electron detection.

Directly accessing the intrinsic two-electron coherence without any HBT contribution can be achieved by partitioning the electronic beam onto a beam splitter in an HBT setup (see Fig. 3). These current correlations are directly related to the inter-channel two-electron coherence right after the beam splitter since fermionic fields within different channels anticommute:

$$\langle i_{1\text{out}}(t_1) i_{2\text{out}}(t_2) \rangle = e^2 v_F^2 \Delta \mathcal{G}_{\text{out}}^{(2e)}(1, t_1; 2, t_2 | 1, t'_1; 2, t'_2) \quad (23)$$

Remarkably, this outgoing two-electron coherence is proportional to the incoming two-electron coherence [14]:

$$\Delta \mathcal{G}_{\text{out}}^{(2e)}(1, t_1; 2, t_2 | 1, t'_1; 2, t'_2) = RT \Delta \mathcal{G}_S^{(2e)}(t_1, t_2 | t'_1, t'_2). \quad (24)$$

Measuring outgoing inter-channel current correlations in the HBT setup thus directly probes the intrinsic excess coherence of the source, as in photon quantum optics.

4.4 Two-particle interferometry as linear filtering Although current correlations in the HBT geometry only give access to the diagonal part of the intrinsic two-electron coherence in the time domain, Eq. (23) naturally leads to a general idea for accessing the off-diagonal part $\Delta \mathcal{G}_S^{(2e)}(t_1, t_2 | t'_1, t'_2)$ for $(t_1, t_2) \neq (t'_1, t'_2)$. The idea is to use linear filters of single-electron coherence as depicted on Fig. 5. Let us assume that the outgoing current is obtained from a linear filtering of the incoming single-electron coherence $\langle i_A \rangle = \mathcal{L}_A [\Delta \mathcal{G}_{\text{lin}}^{(e)}]$ with a similar relation for detector B . Then, the outgoing current correlations $\langle i_A i_B \rangle$ are obtained by applying a linear filter to the

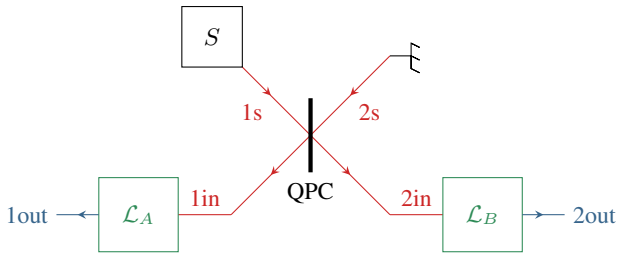


Figure 5 A generalized Franson interferometry experiment: the electron flow emitted by the source S is partitioned at the QPC and sent into two linear filtering components A and B . Current correlations between outgoing currents give access to second-order electronic coherence. Franson interferometry corresponds to using two Mach-Zehnder interferometers for A and B .

incoming two-electron coherence:

$$\langle i_A i_B \rangle = RT \left(\mathcal{L}_A^{(1)} \otimes \mathcal{L}_B^{(2)} \right) \left[\Delta \mathcal{G}_S^{(2e)} \right] \quad (25)$$

in which (24) has been used to obtain (25).

Despite its compactness, Eq. (25) unifies many different experiments under a simple physical interpretation: the intrinsic two-electron coherence $\Delta \mathcal{G}_S^{(2e)}$ describing two-particle excitations emitted by the source, is encoded into current correlations $\langle i_A i_B \rangle$ via an HBT interferometer and two linear filters for single-electron coherence.

In the absence of these filters, the measurement of current correlation gives information on the diagonal part of $\Delta \mathcal{G}_S^{(2e)}$ as seen in section 4.3. When A and B are electronic energy filters, and assuming that no electronic relaxation process takes place between the QPC and the filters (see the discussion in section 3.2), we access the diagonal part of $\Delta \mathcal{G}_S^{(2e)}$ in the frequency domain.

It also naturally leads to the idea of the Franson interferometer [107] originally invented to test photon entanglement [108, 109] and later considered for testing two-particle Aharonov-Bohm effect and electronic entanglement generation [110]. It is a natural way to probe the off-diagonal part of $\Delta \mathcal{G}_S^{(2e)}$ in the time domain since, as explained in section 3.2, a MZI converts single-electron coherences in the time domain into electrical currents.

5 From electron quantum optics to quantum information In this last section, we explain how to relate electron quantum optics quantities to quantum information ones using, once again, signal processing ideas. This enables discussing quantum information quantities in electron quantum optics systems. We illustrate these ideas and procedures by sketching how to get an insight on the many-body state generated by the mesoscopic capacitor.

5.1 Density matrices from electronic coherences

Because electrons are fermions, each single-particle state

can be viewed as a two-level system, thus raising the question of their use as effective qubits to encode quantum information. Given a normalized wavefunction φ_a , its average occupation number is obtained from single-electron coherence by

$$\bar{n}[\varphi_a] = v_F^2 \int_{\mathbb{R}^2} \varphi_a(t_+)^* \varphi_a(t_-) \mathcal{G}_{\rho, x}^{(e)}(t_+ | t_-) dt_+ dt_- \quad (26)$$

where $\varphi_a(t)$ denotes the electronic wavefunction for $x = -v_F t$. The quantity $\bar{n}[\varphi_a]$ being the average value of the number operator $N[\varphi_a] = \psi^\dagger[\varphi_a] \psi[\varphi_a]$, it is between zero and unity. Denoting by $|0_a\rangle$ and $|1_a\rangle$ the states respectively corresponding to the absence or the presence of an electron in the single particle state φ_a , \bar{n}_a and $1 - \bar{n}_a$ can be used as diagonal elements of a 2×2 matrix. However, in the absence of superconductors, charge conservation leads to a superselection rule forbidding quantum superpositions of states of different charges: its off-diagonal elements, which are equal to $\langle \psi^\dagger[\varphi_a] \rangle_\rho$ and its complex conjugate, vanish. Nevertheless, this idea becomes more interesting when considering more than one single-particle state because the various superselection sectors are no longer one dimensional.

A first possibility to obtain an effective qubit is to consider two orthogonal single-particle states φ_a and φ_b and the charge one sector. The basis vector $|0\rangle$ (resp. $|1\rangle$) then corresponds to the state where the electron is totally localized in the electronic state φ_a (resp. φ_b). The reduced density matrix for this railroad electronic qubit [111] is then defined from single and two electron coherences by:

$$\langle 0 | \rho_{\text{qb}} | 0 \rangle = \langle \psi^\dagger[\varphi_a] \psi[\varphi_a] \psi[\varphi_b] \psi^\dagger[\varphi_b] \rangle_\rho \quad (27a)$$

$$\langle 1 | \rho_{\text{qb}} | 1 \rangle = \langle \psi^\dagger[\varphi_b] \psi[\varphi_b] \psi[\varphi_a] \psi^\dagger[\varphi_a] \rangle_\rho \quad (27b)$$

$$\langle 0 | \rho_{\text{qb}} | 1 \rangle = \langle \psi^\dagger[\varphi_a] \psi[\varphi_b] \rangle_\rho \quad (27c)$$

This framework can be extended to situations involving more single-particle states. For example, one could consider two pairs of single-electron states $\varphi_{a1}, \varphi_{a2}$ and $\varphi_{b1}, \varphi_{b2}$ as in the four leads device considered by Samuelsen and Büttiker [112]. The two-particle sector would then contain an effective 2-qubit reduced density matrix whose matrix elements can be expressed in terms of electronic coherences.

Deriving an effective two-qubit reduced density operator from electron coherences directly enables us to use the results from quantum information on the characterization of entanglement in a bipartite system.

Entanglement is well defined and easily characterized for bipartite systems in a pure state using for example the von Neumann entropy of the reduced density matrix of one of the two subsystems [113]. In cases where the whole system is not in a pure state, its total density matrix is said to represent an entangled state if and only if it is not factorized, that is, if and only if it cannot be written as a statistical mixture of tensor products of density operators relative to

each subsystem. In the case of a two qubit system, a single quantity called the concurrence can be used to characterize entanglement. Denoting by $\rho_{2\text{qb}}$ the total density matrix for the two qubits, the concurrence is defined by [114]:

$$C[\rho_{2\text{qb}}] = \max(0, \lambda_1 - \lambda_2 - \lambda_3 - \lambda_4) \quad (28)$$

where $\lambda_1 \geq \lambda_2 \geq \lambda_3 \geq \lambda_4$ are the eigenvalues of the hermitian matrix $R = \sqrt{\sqrt{\rho_{2\text{qb}}} \cdot \tilde{\rho}_{2\text{qb}} \cdot \sqrt{\rho_{2\text{qb}}}}$, and

$$\tilde{\rho}_{2\text{qb}} = (\sigma^y \otimes \sigma^y) \rho_{2\text{qb}}^* (\sigma^y \otimes \sigma^y). \quad (29)$$

The concurrence vanishes if and only if the 2-qubit state is factorized.

The entanglement of formation represents the minimum of the average entanglement of an ensemble of pure states representing $\rho_{2\text{qb}}$ [115]. It corresponds to the minimal number of maximally entangled qubits per realization² needed to generate the entangled states described by $\rho_{2\text{qb}}$ [116, 117]. Remarkably, for a 2-qubit, it has a closed expression in terms of the concurrence [115]:

$$\mathcal{E}[\rho_{2\text{qb}}] = H_2 \left(\frac{1 + \sqrt{1 - C[\rho_{2\text{qb}}]^2}}{2} \right) \quad (30a)$$

$$H_2(x) = -x \log_2(x) - (1-x) \log_2(1-x) \quad (30b)$$

These considerations describe how to obtain quantum information quantities from electron quantum optics concepts. Let us now illustrate these ideas on the study of electron/hole entanglement generated by the mesoscopic capacitor.

5.2 Electron/hole entanglement from the mesoscopic capacitor The mesoscopic capacitor depicted on Fig. 6 is a quantum RC circuit [51] which can be operated in the non-linear regime with a periodic square drive at frequency $f = 1/T$ in order to emit a single-electron excitation during the half period $[0, T/2]$ and a single hole excitation during the second half period $[T/2, T]$ [8]. Reaching this optimal single-electron source regime requires tuning the QPC transparency D (see Fig. 6) so that the electron and hole excitations have the time to form and escape during their respective half periods.

The source is modeled as a time-dependent single-electron scatterer which amounts to neglecting the effect of Coulomb interactions within the dot. Under this hypothesis, the single-electron coherence can be computed using Floquet's theory [72, 118]. Note that in this case, single-electron coherence determines all the electronic coherences emitted by the source since Wick's theorem is valid. Here we use a Floquet description of [98] to obtain the single-electron coherence generated by the mesoscopic

² As often in quantum information, we are looking for the number of maximally entangled pairs needed to generate n copies of the states contained in ρ . For large n , this scales as n and we divide by n to obtain the entanglement of formation.

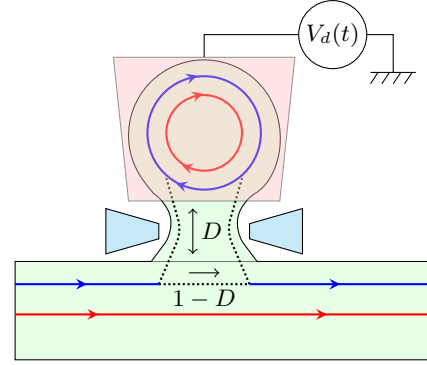


Figure 6 The mesoscopic capacitor consists of a quantum dot with level spacing Δ connected by a QPC (in light blue) to an edge channel (here the outer one in a $\nu = 2$ system). D denotes the transmission probability of the dot so that $D = 1$ corresponds to the case where the dot is totally open and $D = 0$ to the case where the dot is disconnected from the edge channel. Electrons within the dot experience the time-dependent drive potential $V_d(t)$ imposed by a top gate (in light pink). For a square ac voltage at frequency f with zero average and amplitude Δ/e , there exist an optimal value D_{opt} function of Δ/hf for single-electron and hole emission.

capacitor. A program written in C computes the single-electron coherence in the frequency domain. An Haskell code then computes 2-qubit matrices and quantum information theoretical quantities from these data.

We have considered the mesoscopic capacitor with the following experimentally relevant parameters: $\Delta/hf = 20$. The drive voltage $V_d(t)$ is a square voltage. The optimal operation point with these parameters is found to be at $D_{\text{opt}} \simeq 0.35$.

Figure 7 presents the electronic Wigner distribution defined by Eq. (4) for $D = 0.9$, $D \simeq D_{\text{opt}}$ and $D = 0.1$. These plots clearly show that when the dot is fully open, energy resolution is lost, whereas at $D \simeq D_{\text{opt}}$, we clearly see the single-electron and single-hole excitations emitted during each half period. Decreasing D leads to two phenomena: first of all, the length of the electronic wavepacket increases and we see horizontal interference fringes between two-electronic emissions which suggests delocalization of the electronic excitation beyond the time interval $[0, T]$ (same for the hole). We also see interference fringes between the electronic and hole contributions which correspond to an increase of the weight of $\Delta\mathcal{G}_S^{(e)}$ in the electron/hole coherence quadrant in the frequency domain [101]. It was suggested in [98] that, in this regime, during each period, the source emits a state of the form $|\Psi_{eh}(u, v)\rangle = (u + v \psi[\varphi_h] \psi^\dagger[\varphi_e])|F\rangle$ where φ_e and φ_h respectively denote the electronic and hole excitations and (u, v) complex amplitudes such that $|u|^2 + |v|^2 = 1$. At the optimal point $(u, v) \simeq (0, 1)$ whereas $(u, v) \simeq (1, 0)$

when $D \rightarrow 0^+$ since the source is shut down in this limit. Consequently, we have $|u|^2 \simeq |v|^2 \simeq 1/2$ for some intermediate value. In the latter case, this state contains a quantum superposition between the presence and the absence of an elementary electron/hole pair excitation in the edge channel.

Elaborating on section 5.1, we will now test this idea by quantifying the amount of entanglement for an effective 2-qubit built from an electronic and a hole excitation. For this purpose, we define a 4×4 matrix $\rho_{e/h}$ built from states $|x_h x_e\rangle$ associated with the occupation number $x_h \in \{0, 1\}$ for a hole excitation based on the single-particle wavefunction φ_h and the electronic occupation number $x_e \in \{0, 1\}$ associated with the single-particle state φ_e . All matrix elements that couple different charge sectors vanish. The remaining matrix elements are the diagonal ones:

$$\langle 00 | \rho_{e/h} | 00 \rangle = \langle \psi^\dagger[\varphi_h] \psi[\varphi_h] \psi[\varphi_e] \psi^\dagger[\varphi_e] \rangle_\rho \quad (31a)$$

$$\langle 01 | \rho_{e/h} | 01 \rangle = \langle \psi^\dagger[\varphi_h] \psi[\varphi_h] \psi^\dagger[\varphi_e] \psi[\varphi_e] \rangle_\rho \quad (31b)$$

$$\langle 10 | \rho_{e/h} | 10 \rangle = \langle \psi[\varphi_h] \psi^\dagger[\varphi_h] \psi[\varphi_e] \psi^\dagger[\varphi_e] \rangle_\rho \quad (31c)$$

$$\langle 11 | \rho_{e/h} | 11 \rangle = \langle \psi[\varphi_h] \psi^\dagger[\varphi_h] \psi^\dagger[\varphi_e] \psi[\varphi_e] \rangle_\rho \quad (31d)$$

and the off-diagonal elements coupling the state $|00\rangle$ to the state $|11\rangle$:

$$\langle 11 | \rho_{e/h} | 00 \rangle = \langle \psi^\dagger[\varphi_h] \psi[\varphi_e] \rangle_S. \quad (32)$$

The diagonal matrix elements (31) are all related to the two-electron coherence $\bar{n}[\varphi_e, \varphi_h]$ whereas the off-diagonal ones are directly the single-electron coherence in the electron/hole coherence quadrant $\mathcal{G}_S^{(e)}[\varphi_e | \varphi_h] = \text{Tr}(\psi[\varphi_e] \rho \psi^\dagger[\varphi_h])$.

When Wick's theorem is valid, which is the case in our Floquet modelization of the mesoscopic capacitor, we have:

$$\langle 00 | \rho_{e/h} | 00 \rangle = (1 - \bar{n}_e) \bar{n}_h + |\xi|^2 \quad (33a)$$

$$\langle 01 | \rho_{e/h} | 01 \rangle = \bar{n}_e \bar{n}_h - |\xi|^2 \quad (33b)$$

$$\langle 10 | \rho_{e/h} | 10 \rangle = (1 - \bar{n}_e)(1 - \bar{n}_h) - |\xi|^2 \quad (33c)$$

$$\langle 11 | \rho_{e/h} | 11 \rangle = \bar{n}_e(1 - \bar{n}_h) + |\xi|^2 \quad (33d)$$

where $\xi = \langle 11 | \rho_{e/h} | 00 \rangle = \mathcal{G}_S^{(e)}[\varphi_e | \varphi_h]$ is the electron/hole coherence between the electronic and hole wavefunctions and $\bar{n}_{e/h} = \bar{n}[\varphi_{e/h}]$ are their occupation numbers. The Cauchy-Schwarz inequality tells us that

$$\left| \mathcal{G}_S^{(e)}[\varphi_e | \varphi_h] \right|^2 \leq \bar{n}_e \bar{n}_h. \quad (34)$$

When the bound is saturated, the matrix $\rho_{e/h}$ gets a zero on the diagonal and, in this case, the concurrence can be evaluated analytically:

$$\mathcal{C}[\rho_{e/h}] = 2\sqrt{\bar{n}_e \bar{n}_h}. \quad (35)$$

It is non zero when we are away from the single-electron source regime ($\bar{n}_e = 1$ and $\bar{n}_h = 0$). In particular for the state $|\Psi_{e/h}(u, v)\rangle$ which can be shown to satisfy Wick's theorem, considering $|u|^2 = |v|^2 = 1/2$ gives $\bar{n}_e = \bar{n}_h = 1/2$ and thus $\mathcal{C} = 1$. Then, $\mathcal{E}[\rho_{e/h}] = 1$, as expected since, in this case, we are producing a pure state with electron/hole entanglement.

However, for arbitrary electronic and hole wavepackets $\varphi_{e/h}$, the reduced density operator $\rho_{e/h}$ may not be so ideal. We shall now discuss which wavepackets are the best candidates for obtaining non-zero concurrence.

5.3 Numerical results As we shall see now, the choice of $\varphi_{e/h}$ has a strong influence on the result. At fixed \bar{n}_e and \bar{n}_h , the concurrence is maximal for ξ saturating the Cauchy-Schwarz bound (34) but its value can be very small when $\bar{n}_e \simeq 0$ and $\bar{n}_h \simeq 1$. We thus have to find wavepackets which (i) bring \bar{n}_e and \bar{n}_h as close as possible to 1/2 and (ii) maximize $|\mathcal{G}_S^{(e)}[\varphi_e | \varphi_h]|$.

A first guess for φ_e is a truncated Lorentzian in energy, centered at $\hbar\omega_e = \Delta/2$ and whose width fits the exponential decay of the average current. Note that its natural width γ_e depends on D . This wavepacket is expected to lead to $\bar{n}_e \simeq 1$ when $D = D_{\text{opt}}$. In this case, the natural width of the wavepacket should be less than a half period. However, when $D \rightarrow 0$, it may be relevant to consider electronic wavepackets delocalized over more than one period. Our ansatz is to consider the product of the truncated Lorentzian in energy with a characteristic function in time that selects n half-periods during which the electron is emitted ($t \in [lT, (l + 1/2)T]$ for $l = 0, \dots, n - 1$). Truncation in the time domain implies that our ansatz are not anymore a purely electronic state. In order to ensure this, we set to zero all values at negative frequencies. This implies that the wavepackets we consider are not strictly zero in time outside of $[lT, (l + 1/2)T]$. However, when $D \leq D_{\text{opt}}$ the excitations are emitted at well separated energies $\hbar\omega_{e/h} = \pm\Delta/2$ with respect to their natural width $\hbar\gamma_e$, so contributions outside these half periods are very small (and indeed smaller as D decreases). When $D \geq D_{\text{opt}}$, the natural width of the excitation decreases, ensuring it is less than a half period. After normalization, this defines wavefunctions φ_{e_n} and in the same way wavefunctions φ_{h_n} .

We present on Fig. 8 the quantities $\bar{n}_{e/h}$, the modulus of the electron/hole coherence $|\xi|$, the Cauchy-Schwarz bound and the von Neumann entropy of the 2-qubit matrix $\rho_{e/h}$ using specific couples of electronic and hole wavefunctions. We consider φ_{e_n} and φ_{h_n} for $n = 1$, *id est* truncated to one half period and thus denoted by ‘‘Truncated’’ on Figs. 8 and 9 and also $n = \infty$ which corresponds to the ‘‘Delocalized’’ wavefunctions over many half periods.

The von Neumann entropy of the 2-qubit density matrices obtained from these two wavepacket families shows roughly the same behavior for $D \gtrsim 0.1$. First of all, it never vanishes for $D \neq 0$ thus showing that $\rho_{e/h}$ does not represent a rank one projector. The von Neumann entropy goes

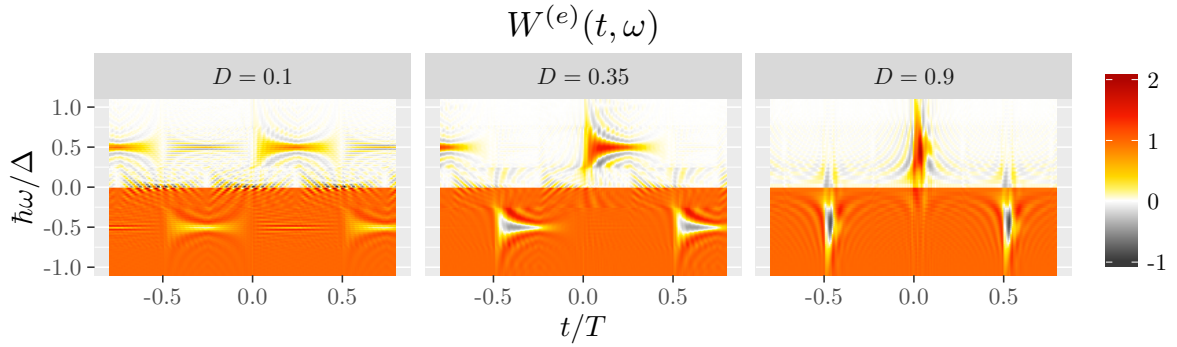


Figure 7 The electronic Wigner function $W^{(e)}(t, \omega)$ for the mesoscopic capacitor operated at the electron/hole symmetric point and driven by a square potential of amplitude Δ/e at frequency f such that $\Delta/hf = 20$. Plots are presented for $D = 0.1$, $D = D_{\text{opt}} \approx 0.35$ and $D = 0.9$.

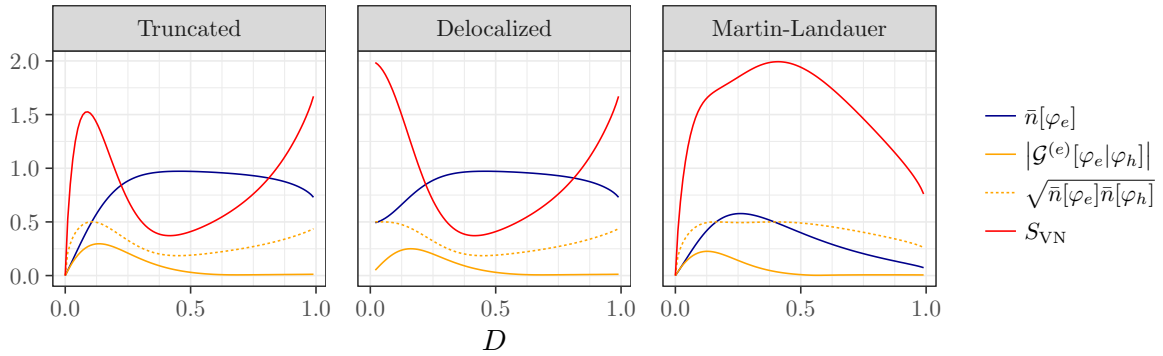


Figure 8 The average occupation \bar{n}_e (blue line), the modulus of the coherence $|\mathcal{G}_S^{(e)}[\varphi_e|\varphi_h]|$ (orange line), the Cauchy-Schwarz bound $\sqrt{\bar{n}_e\bar{n}_h}$ (dashed orange line) and the von Neumann entropy S_{VN} of $\rho_{e/h}$ (red line) as functions of D for the three families of wavepackets “Truncated”, “Delocalized” and “Martin Landauer”. The mesoscopic capacitor is operated with the parameters used for Fig. 7.

through a minimum close to D_{opt} and then re-increases. This comes from the fact that these wavepackets are indeed well suited to describe the excitations emitted by the mesoscopic capacitor around the optimal regime as attested by the fact that $\bar{n}_e \simeq 1$ for this regime.

In the vanishing D limit, $\bar{n}_e \approx 0.50$ for the delocalized wavepacket whereas $\bar{n}_e \rightarrow 0$ for the truncated ones. This reflects the delocalization over more than one half period of the electronic excitations when $D \rightarrow 0$. For the delocalized wavepackets, the Cauchy-Schwarz bound is not saturated when $D \rightarrow 0$. The effective 2-qubit density matrix $\rho_{e/h}$ thus becomes diagonal. Due to the non-vanishing limit of \bar{n}_e when $D \rightarrow 0$, the von Neumann entropy remains close to 2 (which would be obtained for $\xi = 0$ and $\bar{n}_e = \bar{n}_h = 1/2$). By contrast, for the truncated wavepackets, \bar{n}_e goes to 0 and $\bar{n}_h \rightarrow 1$ when $D \rightarrow 0$. The Cauchy-Schwarz bound is also not saturated. In this case, $\rho_{e/h}$ collapses onto a matrix

with only one non-zero element on its diagonal: the von Neumann entropy decreases when $D \rightarrow 0$ for truncated wavepackets.

The concurrence as a function of D is depicted on Fig. 9. We see that for delocalized wavepackets, $\rho_{e/h}$ exhibits a non-zero concurrence on a finite interval of D that stops before D gets close to zero and starts a little before D_{opt} . The lower limit of the interval where electron/hole entanglement can be observed with the delocalized wavepackets comes from decay of electron/hole coherences as $D \rightarrow 0$. Although these wavepackets tend to be quite good in terms of their overlaps with $\mathcal{G}_S^{(e)}$, the coherence is too small to get a non-zero entanglement. For the truncated wavepacket, the concurrence is higher than for delocalized wavepackets as $D \rightarrow 0$ as expected since it is only for small D that these two wavepackets become significantly different.

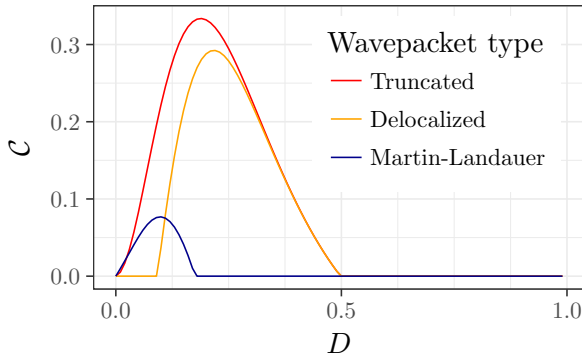


Figure 9 The concurrence $C[\rho_{eh}]$ as function of D for the three families of wavepackets “Truncated”, “Delocalized” and “Martin Landauer”. The mesoscopic capacitor is operated with the parameters used for Fig. 7.

Although this numerical investigation shows that the mesoscopic capacitor generates some electron/hole pair entanglement in the low D limit, it also shows the importance of using the proper single-particle states to study quantum information theoretical quantities and also to probe the many-body nature of the electronic fluid. We will now sketch a general strategy inspired by signal processing for analyzing electronic coherences generated by a time-periodic source.

5.4 Electronic atoms of signal The above discussion was based on the use of empirical electron and hole wavefunctions without thinking of any detection scheme. However, for a T -periodic source, one could envision time-dependent detectors ideally performing repeated detections of a given single-particle template across various periods. Although this is still not demonstrated experimentally, it is important to develop a signal processing framework for the corresponding signals.

The idea, borrowed from M. Devoret’s lectures at Collège de France [119] consists in using a family of single-particle wavefunctions well suited to T -periodicity. We thus consider single-particle wavepackets $\varphi_{k,l}$, which we call electronic atoms of signal or, adapting M. Devoret’s terminology, electronic wavelets such that

$$\varphi_{k,l}(t) = \varphi_k(t - lT) \quad (36a)$$

$$\langle \varphi_{k',l'} | \varphi_{k,l} \rangle = \delta_{k,k'} \delta_{l,l'}. \quad (36b)$$

Families $\varphi_{k,l}$ obtained by translations in both the frequency and time domains arising from a single wavepacket $\varphi_{0,0}$ are called Gabor bases. An important result for Gabor bases is the Balian-Low theorem which states that there is no orthogonal basis of this type that is well localized both in the time and frequency domain. In the signal processing community, discrete wavelets are families satisfying (36) in which the parameter k corresponds to a scaling: $\varphi_{k,l}(t) = (v_F \tau_0)^{-1/2} s^{-k/2} \varphi((t/s^n - lT)/\tau_0)$.

A famous example of electronic atoms of signal has been introduced by Th. Martin and R. Landauer [18]. These wavepackets with energy bandwidth hf ($f = 1/T$) are defined by:

$$\varphi_{n,l=0}(t) = \frac{1}{\sqrt{v_F T}} \frac{\sin(\pi f t)}{\pi f t} e^{-i\omega_n t} \quad (37)$$

where $\omega_n = \pi f(2n + 1/2)$. They are called Shannon wavelets in the signal processing community. Remarkably, when a voltage drive of period T is applied, the single-particle state $\varphi_{n,l}$ is scattered among the $\varphi_{n',l}$ with the same time slot index l [9].

More recently, M. Moskalets has found a family of mutually orthogonal electronic wavepackets $(\varphi_l)_{l \in \mathbb{Z}}$ respectively time-shifted by lT and such that a train of single-electron Leviton excitations is represented as the infinite Slater determinant of these φ_l on top of the Fermi sea [120]. It is then tempting to conjecture that there exists a family of electronic atoms of signal $\varphi_{n,l}$ satisfying the orthogonality condition (36b) such that a train of charge n Levitons is obtained as the infinite Slater determinant formed by the $\varphi_{k,l}$ for $l \in \mathbb{Z}$ and $k = 1, \dots, n$ on top of the Fermi sea.

Electronic atoms of signal can be used to model repeated detection of φ_k by considering the overlap of the single-electron coherence of a T -periodic source S with a train of N wavepackets $\varphi_{k,l}$ where k is fixed and $l = 1, \dots, N$. This overlap represents the average cumulated signal after N successive detections of the wavepacket φ_k shifted by multiples of T . Due to the orthogonality of the $\varphi_{k,l}$ for different values of l , these time-shifted wavepackets are perfectly distinguishable: the corresponding number operators $N[\varphi_{k,l}]$ and $N[\varphi_{k,l'}]$ commute. Using the T periodicity of $\mathcal{G}_S^{(e)}$, this overlap scales as N with a prefactor $\bar{n}[\varphi_k]$ defined by Eq. (26). The same reasoning can be extended to two-particle detection. We then consider φ_a and φ_b for $a \neq b$ and we perform a repeated detection of the electron pair. The associated wavefunctions are the normalized Slater determinants $\varphi_{(a,b;l)}(t_1, t_2)$ built from $\varphi_{a,l}$ and $\varphi_{b,l}$ for $l = 1, \dots, N$. Exactly as in the single-particle detection, due to orthogonality of the single-particle wavefunctions for $l \neq l'$, the two-particle states $\varphi_{(a,b;l)}$ are orthogonal for different values of l . The cumulated average signal for N periods is then the overlap of $\mathcal{G}^{(2e)}$ with the sum over l of $\varphi_{(a,b;l)}(t_1^+, t_2^+) \varphi_{(a,b;l)}(t_1^-, t_2^-)^*$. Once again this overlap scales as N with a prefactor $\bar{n}[\varphi_a, \varphi_b]$ equal to

$$v_F^4 \int_{\mathbb{R}^4} \varphi_{(a,b)}(\mathbf{t}_+)^* \varphi_{(a,b)}(\mathbf{t}_-) \mathcal{G}_S^{(2e)}(\mathbf{t}_+ | \mathbf{t}_-) d^2 \mathbf{t}_+ d^2 \mathbf{t}_-. \quad (38)$$

Through repeated detections of the same wavefunction in different time slots, electronic atoms of signal thus enable us to define effective density matrices in the basis of occupation number for orthogonal single-particle levels.

To illustrate this point, Figs. 8 and 9 also present the same results as before but for Martin Landauer electronic

atoms of signals associated with the period $T/2$ so that φ_e is centered in energy at ω_e and in time on the first half period and φ_h is centered in energy at ω_h and in time on the second half period. As can be seen from the behavior of \bar{n}_e , these atoms of signals are not well suited close to D_{opt} . This was expected since their energy width $2hf$ is less than the natural width of the emitted single-electron excitation. However, the electron/hole coherence ξ is closer to the Cauchy-Schwarz bound than the truncated and delocalized wavepackets. As a result, the non-vanishing interval for the concurrence is indeed concentrated at lower values than for the truncated and delocalized wavepackets.

What we are doing here is to analyze the fermionic analogue of inter-mode entanglement in quantum optics. Considering various families of single-particle state amounts to considering various pairs of modes. Naturally, quantum information quantities measuring this entanglement depend on the modes considered. This raises the question of the best description of a quantum signal such as single-electron coherence in terms of single-particle wavefunctions. What are the guidelines for such a choice? Although we do not have a definitive answer to this very general question, we think there are two ways of addressing it.

First of all, the experimental setup may impose us a choice. For example, Moskalets wavefunctions and their conjectural generalization are the natural choice when discussing an HOM experiment with a source emitting a periodic train of Leviton excitations in one of the incoming channels. Next, when starting from computational or experimental data on single-electron coherence, the problem is to determine atoms of signals or other wavepackets giving the “simplest” description of single-electron coherence. Although answering this question goes beyond the scope of the present paper, methods inspired from signal processing and exploiting the T -periodicity of single-electron coherence are certainly worth investigating.

6 Conclusion and perspectives In this paper, we have discussed the recent developments in electron quantum optics from a signal processing perspective. Although part of the material presented here forms a review of our recent works in electron quantum optics [1, 14, 24, 39, 40], our discussion aims at showing new interesting perspectives for future work as well as connections to other topics such as quantum optics of current noise or the study of quantum information quantities in electronic systems.

From that perspective, our first main message is that single- and two-particle interferometry experiments can be interpreted in the signal processing language as analog operations converting “quantum signals” such as single- and two-electron coherences into experimentally observable quantities which are zero- or finite-frequency average current and current correlations. In particular, we have reviewed how the HOM experiment encodes the overlap of single-electron coherences within low-frequency current noise, thus giving more substance to Landauer’s aphorism

“The noise is the signal” [121]. We have also shown that the signal processing point of view is relevant beyond the analysis of HOM experiments. For example, it also unifies the direct probing of intrinsic two-electron coherence within a given edge channel by means of generalized Franson interferometry experiments.

Our approach thus suggests that, although the demonstration of a Franson interferometer in electron quantum optics represents a strong challenge due to interaction effects within Mach-Zehnder interferometers, it might be easier to probe two-electron coherences with a simple Hanbury Brown and Twiss interferometer by measuring correlations between finite-frequency currents. Although this would require sophisticated homodyning to bring the finite-frequency components of both outgoing currents in the same low-frequency band, the measurement stage would be rather immune to interaction effects. Interestingly, this would also establish a bridge between electron quantum optics and the recently developed study of quantum properties of the radiation emitted by a quantum conductor [29].

Our second message is that signal processing concepts and techniques are useful not only for interpreting electron quantum optics experimental results but also to gain a deeper understanding of the electronic many-body state in these experiments.

For this purpose, we have transposed the concept of atoms of signal to electron quantum optics and shown that it can be used to discuss quantum information theory quantities in electron quantum optics experiments. We have illustrated this idea by discussing the electron/hole entanglement generated by the mesoscopic capacitor. However, our discussion is relevant to the study of entanglement in more general setups (see for example [122] in this volume and [123, 124] as well as [46, 125, 126, 127, 128, 129, 130] for previous works). By relying only on the use of electron quantum optics coherences, our framework enables discussing Coulomb interaction effects in a very natural way. Second, we think that the pioneering work by M. Moskalets on Leviton trains [120] raises the question of the “simplest representation” of quantum signals such as single-electron coherences emitted by various electronic sources. We think that combining the arsenal of theoretical techniques (analytical as well as numerical) with signal processing concepts may lead to progresses on this basic question.

Last but not least, the rapid development of experiments in electron quantum optics and microwave quantum optics suggests that the perspectives for investigating all these questions on the experimental side are very promising.

Acknowledgements We warmly thank J. Splettstoesser and R. Haug for setting up this special volume. We acknowledge useful discussions with P. Borgnat and R. Menu. This work was supported by the ANR grants “Ishot reloaded” (Grant No. ANR-

14-CE32-0017) and by the ERC consolidator grant “EQuO” (Grant No. 648236).

References

- [1] E. Bocquillon, V. Freulon, F. Parmentier, J.M. Berroir, B. Plaçais, C. Wahl, J. Rech, T. Jonckheere, T. Martin, C. Grenier, D. Ferraro, P. Degiovanni, and G. Fève, *Ann. Phys. (Berlin)* **526**, 1–30 (2014).
- [2] M. Henny, S. Oberholzer, C. Strunk, T. Heinzel, K. Ensslin, M. Holland, and C. Schönberger, *Science* **284**, 296 (1999).
- [3] W. Oliver, J. Kim, R. Liu, and Y. Yamamoto, *Science* **284**, 299 (1999).
- [4] Y. Blanter and M. Büttiker, *Physics Reports* **336**, 1 (2000).
- [5] Y. Ji, Y. Chung, D. Sprinzak, M. Heiblum, D. Mahalu, and H. Shtrikman, *Nature* **422**, 415 (2003).
- [6] I. Neder, M. Heiblum, D. Mahalu, and V. Umansky, *Phys. Rev. Lett.* **98**, 036803 (2007).
- [7] I. Neder, N. Ofek, Y. Chung, M. Heiblum, D. Mahalu, and V. Umansky, *Nature* **448**, 333 (2007).
- [8] G. Fève, A. Mahé, J.M. Berroir, T. Kontos, B. Plaçais, D.C. Glattli, A. Cavanna, B. Etienne, and Y. Jin, *Science* **316**, 1169 (2007).
- [9] J. Dubois, T. Jullien, C. Grenier, P. Degiovanni, P. Roulleau, and D. C. Glattli, *Phys. Rev. B* **88**, 085301 (2013).
- [10] L. Levitov, H. Lee, and G. Lesovik, *J. Math. Phys.* **37**, 4845 (1996).
- [11] C. Grenier, R. Hervé, G. Fève, and P. Degiovanni, *Mod. Phys. Lett. B* **25**, 1053 – 1073 (2011), Proceedings of the Statphys 24 satellite meeting “International Conference on Frustrated Spin Systems, Cold Atoms and Nanomaterials” (Hanoi, 14-16 July 2010).
- [12] G. Haack, M. Moskalets, and M. Büttiker, *Phys. Rev. B* **87**(201302(R)) (2012).
- [13] M. Moskalets, *Phys. Rev. B* **89**, 045402 (2014).
- [14] E. Thibierge, D. Ferraro, B. Roussel, C. Cabart, A. Marguerite, G. Fève, and P. Degiovanni, *Phys. Rev. B* **113**, 081302(R) (2016).
- [15] R. Landauer and M. Büttiker, *Phys. Rev. Lett.* **54**, 2049–2053 (1985).
- [16] M. Büttiker, Y. Imry, R. Landauer, and S. Pinhas, *Phys. Rev. B* **31**, 6207 – 6215 (1985).
- [17] M. Büttiker, *Phys. Rev. Lett.* **57**, 1761 (1986).
- [18] T. Martin and R. Landauer, *Phys. Rev. B* **45**, 1742 – 1755 (1992).
- [19] M. Büttiker, *Phys. Rev. B* **46**, 12485 – 12507 (1992).
- [20] M. Büttiker, A. Prêtre, and H. Thomas, *Phys. Rev. Lett.* **70**, 4114 (1993).
- [21] A. Prêtre, H. Thomas, and M. Büttiker, *Phys. Rev. B* **54**, 8130 (1996).
- [22] T. Christen and M. Büttiker, *Phys. Rev. B* **53**, 2064 (1996).
- [23] D. Pines and P. Nozières, *The theory of quantum liquids* (Perseus Book, 1966).
- [24] A. Marguerite, E. Bocquillon, J.M. Berroir, B. Plaçais, and G. Fève, Two-particle interferometry in quantum Hall edge channels, To appear in the present volume: DOI:10.1002/pssb.201600618 (2016).
- [25] C. Eichler, D. Bozyigit, C. Lang, L. Steffen, J. Fink, and A. Wallraff, *Phys. Rev. Lett.* **106**, 220503 (2011).
- [26] C. Lang, C. Eichler, L. Steffen, J. Fink, M. Woolley, A. Blais, and A. Wallraff, *Nature Physics* **9**, 345 (2013).
- [27] D. Bozyigit, C. Lang, L. Steffen, J.M. Fink, C. Eichler, M. Baur, R. Bianchetti, P.J. Leek, S. Filipp, M.P. da Silva, A. Blais, and A. Wallraff, *Nat Phys* **7**, 154–158 (2011).
- [28] C. Beenakker and H. Schomerus, *Phys. Rev. Lett.* **93**, 096801 (2004).
- [29] A. Grimsmo, F. Qassemi, B. Reulet, and A. Blais, *Phys. Rev. Lett.* **116**, 043602 (2015).
- [30] U. Mendes and C. Mora, *New Journal of Physics* **17**, 11 (2015).
- [31] J. Forgues, C. Lupien, and B. Reulet, *Phys. Rev. Lett.* **113**, 043603 (2014).
- [32] J. Forgues, C. Lupien, and B. Reulet, *Phys. Rev. Lett.* **114**, 130403 (2015).
- [33] K. Thibaut, J. Gabelli, C. Lupien, and B. Reulet, *Phys. Rev. Lett.* **114**, 236604 (2015).
- [34] S. Virally, J.O. Simoneau, C. Lupien, and B. Reulet, *Phys. Rev. A* **93**, 043813 (2016).
- [35] J. Moura, *IEEE Signal Processing Magazine* **26**, 6 (2009).
- [36] E. Bocquillon, V. Freulon, J.M. Berroir, P. Degiovanni, B. Plaçais, A. Cavanna, Y. Jin, and G. Fève, *Science* **339**, 1054 (2013).
- [37] T. Jullien, P. Roulleau, B. Roche, A. Cavanna, Y. Jin, and D. C. Glattli, *Nature* **514**(10), 603–607 (2014).
- [38] V. Freulon, A. Marguerite, J.M. Berroir, B. Plaçais, A. Cavanna, Y. Jin, and G. Fève, *Nature Communications* **6**, 6854 (2015).
- [39] A. Marguerite, C. Cabart, C. Wahl, B. Roussel, V. Freulon, D. Ferraro, C. Grenier, J.M. Berroir, N. Plaçais, T. Jonckheere, J. Rech, T. Martin, P. Degiovanni, A. Cavanna, Y. Jin, and G. Fève, *Phys. Rev. B* **94**, 115311 (2016).
- [40] D. Ferraro, A. Feller, A. Ghibaud, E. Thibierge, E. Bocquillon, G. Fève, C. Grenier, and P. Degiovanni, *Phys. Rev. B* **88**, 205303 (2013).
- [41] D. Wharam, M. Petter, H. Ahmed, J. Frost, D. Hasko, D. Peacock, D. Richie, and G. Jones, *Journal of Physics C: Solid State Physics* **21**, L887 (1988).
- [42] B. J. van Wees, H. van Houten, C. W. J. Beenakker, J. G. Williamson, L. P. Kouwenhoven, D. van der Marel, and C. T. Foxon, *Phys. Rev. Lett.* **60**, 848–850 (1988).
- [43] H. van Houten, C. Beenakker, and B. van Wees, *Quantum Point Contacts, Semiconductors and semimetals*, Vol. 35, (Academic Press, 1992), chap. 2.
- [44] P. Roulleau, F. Portier, D.C. Glattli, P. Roche, A. Cavanna, G. Faini, U. Gennser, and D. Mailly, *Phys. Rev. B* **76**, 161309 (2007).
- [45] P. Roulleau, F. Portier, P. Roche, A. Cavanna, G. Faini, U. Gennser, and D. Mailly, *Phys. Rev. Lett.* **101**, 186803 (2008).
- [46] P. Samuelsson, E. Sukhorukov, and M. Büttiker, *Phys. Rev. Lett.* **92**, 026805 (2004).
- [47] P. Roulleau, F. Portier, D.C. Glattli, P. Roche, A. Cavanna, G. Faini, U. Gennser, and D. Mailly, *Phys. Rev. Lett.* **100**, 126802 (2008).

- [48] M.D. Blumenthal, B. Kaestner, L. Li, S. Giblin, T.J.B.M. Janssen, M. Pepper, D. Anderson, G. Jones and D.A. Ritchie, *Nature Physics* **3**, 343 (2007).
- [49] J.D. Fletcher, P. See, H. Howe, M. Pepper, S.P. Giblin, J.P. Griffiths, G.A.C. Jones, I. Farrer, D.A. Ritchie, T.J.B.M. Janssen, and M. Kakatoa, *Phys. Rev. Lett* **111**, 216807 (2013).
- [50] D.C. Glattli and P. Roulleau, Levitons for electron quantum optics. To appear in this volume: DOI:10.1002/pssb.201600650 (2016).
- [51] J. Gabelli, G. Fève, J.M. Berroir, B. Plaçais, A. Cavanna, B. Etienne, Y. Jin, and D.C. Glattli, *Science* **313**, 499 (2006).
- [52] J. Gabelli, G. Fève, T. Kontos, J.M. Berroir, B. Plaçais, D.C. Glattli, B. Etienne, Y. Jin, and M. Büttiker, *Phys. Rev. Lett.* **98**, 166806 (2007).
- [53] M. Büttiker, H. Thomas, and A. Prêtre, *Phys. Lett. A* **180**, 364 (1993).
- [54] C. Gardiner and M. Collett, *Phys. Rev. A* **31**, 3761 (1985).
- [55] D. Ferraro, T. Jonckheere, J. Rech, and T. Martin, Electron quantum optics beyond the integer quantum Hall effect. To appear in the present volume: DOI:10.1002/pssb.201600531 (2016).
- [56] D. Ferraro, J. Rech, T. Jonckheere, and T. Martin, *Phys. Rev. B* **91**, 205409 (2015).
- [57] J. Rech, D. Ferraro, L. Vannucci, M. Sasseti and T. Martin, Minimal excitations in the fractional quantum Hall regime. arXiv:1606.01122.
- [58] P. Fendley, A.W.W. Ludwig and H. Saleur, *Phys. Rev. B* **52**, 8934 (1995).
- [59] B. Karmarkar, D. Venturelli, L. Chirolli, F. Taddei, V. Giovannetti, R. Fazio, S. Roddaro, G. Viasol, L. Sorba, V. Pellegrini and F. Beltram, *Phys. Rev. Lett.* **107**, 236804 (2011).
- [60] M.Z. Hasan and C. Kane, *Rev. Mod. Phys.* **82**, 3045 (2010).
- [61] P. Hofer and M. Büttiker, *Phys. Rev. B* **88**, 241308 (2013).
- [62] A. Inhofer and D. Barcioux, *Phys. Rev. B* **88**, 235412 (2013)
- [63] D. Ferraro, C. Wahl, T. Jonckheere and T. Martin, *Phys. Rev. B* **89**, 075407 (2014).
- [64] G. Dolcetto and T.L. Schmidt, *Phys. Rev. B* **94**, 075444 (2016).
- [65] Y. Xing, Z.L. Yang, Sun, Q.-F. and J. Wang, *Phys. Rev. B* **90**, 075435 (2014).
- [66] E.V. Sukhorukov and V. Cheianov, *Phys. Rev. Lett.* **99**, 156801 (2007).
- [67] A. Calzona, M. Acciai, M. Carrega, F. Cavaliere and M. Sasseti, *Phys. Rev. B* **94**, 035404 (2016).
- [68] R. Glauber, *Phys. Rev.* **130**, 2529 (1963).
- [69] F. Zernicke, *Physica* **5**, 785 (1938).
- [70] G. Haack, M. Moskalets, J. Splettstoesser, and M. Büttiker, *Phys. Rev. B* **84**, 081303 (2011).
- [71] C. Altimiras, H. le Sueur, U. Gennser, A. Cavanna, D. Mailly, and F. Pierre, *Nature Physics* **6**, 34 (2010).
- [72] M. Moskalets, Scattering matrix approach to non-stationary quantum transport (Imperial College Press, London, 2011).
- [73] I. Safi, *Eur. Phys. J. D* **12**, 451 (1999).
- [74] P. Degiovanni, C. Grenier, and G. Fève, *Phys. Rev. B* **80**, 241307(R) (2009).
- [75] B. Yurke, *Phys. Rev. A* **29**, 1419 (1984).
- [76] C. Grenier, J. Dubois, T. Jullien, P. Roulleau, D. C. Glattli, and P. Degiovanni, *Phys. Rev. B* **88**, 085302 (2013).
- [77] D. Ferraro, C. Wahl, J. Rech, T. Jonckheere, and T. Martin, *Phys. Rev. B* **89**, 075407 (2014).
- [78] J. Chalker, Y. Gefen, and M. Veillette, *Phys. Rev. B* **76**, 085320 (2007).
- [79] I. Neder, F. Marquardt, M. Heiblum, D. Mahalu, and V. Umansky, *Nature Physics* **3**, 534 (2007).
- [80] I. Levkivskiy and E. Sukhorukov, *Phys. Rev. B* **78**, 045322 (2008).
- [81] C. Neuenhahn and F. Marquardt, *New Journal of Physics* **10**, 115018 (2008).
- [82] D.L. Kovrizhin and J.T. Chalker, *Phys. Rev. B* **80**, 161306 (2009).
- [83] S. Tewari, P. Roulleau, C. Grenier, F. Portier, A. Cavanna, U. Gennser, D. Mailly, and P. Roche, *Phys. Rev. B* **93**, 035420 (2016).
- [84] A. O. Slobodeniuk, E. G. Idrisov, and E. V. Sukhorukov, *Phys. Rev. B* **93**, 035421 (2016).
- [85] E. Bocquillon, V. Freulon, J. Berroir, P. Degiovanni, B. Plaçais, A. Cavanna, Y. Jin, and G. Fève, *Nature Communications* **4**, 1839 (2013).
- [86] R. Hanbury Brown and R. Twiss, *Nature* **178**, 1046 (1956).
- [87] R. Hanbury Brown and R. Twiss, *Nature* **177**, 27 (1956).
- [88] U. Fano, *Am. J. Phys.* **29**, 539 (1961).
- [89] C. Hong, Z. Ou, and L. Mandel, *Phys. Rev. Lett.* **59**, 2044 (1987).
- [90] G. Baym, *Acta Physical Polonica B* **29**, 1839 (1998).
- [91] T. Jelts, J. McNamara, W. Hogervorst, W. Vassen, V. Krachmalnicoff, M. Schellekens, A. Perrin, C. Hong, D. Boiron, A. Aspect, and C. Westbrook, *Nature* **445**, 402 (2007).
- [92] J. Beugnon, M. Jones, J. Dingjan, B. Darquié, G. Messin, A. Browaeys, and P. Grangier, *Nature* **440**, 779 (2006).
- [93] R. Lopes, A. Imanaliev, A. Aspect, M. Cheneau, D. Boiron, and C.I. Westbrook, *Nature* **520**(7545), 66–68 (2015).
- [94] D. T. Smithey, M. Beck, M. G. Raymer, and A. Faridani, *Phys. Rev. Lett.* **70**, 1244 (1993).
- [95] A. I. Lvovsky and M. G. Raymer, *Rev. Mod. Phys.* **81**, 299–332 (2009).
- [96] A. Ourjoumtsev, R. Tualle-Brouiri, and P. Grangier, *Phys. Rev. Lett.* **96**, 213601 (2006).
- [97] M.P. da Silva, D. Bozyigit, A. Wallraff, and A. Blais, *Phys. Rev. A* **82**, 043804 (2010).
- [98] C. Grenier, R. Hervé, E. Bocquillon, F. Parmentier, B. Plaçais, J.M. Berroir, G. Fève, and P. Degiovanni, *New Journal of Physics* **13**, 093007 (2011).
- [99] E. Bocquillon, F. Parmentier, C. Grenier, J. M. Berroir, P. Degiovanni, D.C. Glattli, B. Plaçais, A. Cavanna, Y. Jin, and G. Fève, *Phys. Rev. Lett.* **108**, 196803 (2012).
- [100] H. Le Sueur, C. Altimiras, U. Gennser, A. Cavanna, D. Mailly, and F. Pierre, *Phys. Rev. Lett.* **105**, 056803 (2010).
- [101] P. Degiovanni, C. Grenier, G. Fève, C. Altimiras, H. le Sueur, and F. Pierre, *Phys. Rev. B* **81**, 121302(R) (2010).

- [102] C. Wahl, J. Rech, T. Jonckheere, and T. Martin, *Phys. Rev. Lett.* **112**, 046802 (2014).
- [103] F. Parmentier, A. Mahé, A. Denis, J.M. Berroir, D.C. Glattli, B. Plaçais, and G. Fève, *Rev. Sci. Instrum.* **82**, 013904 (2011).
- [104] G. Gasse, C. Lupien, and B. Reulet, *Phys. Rev. Lett.* **111**, 136601 (2013).
- [105] J. Ville, *Câbles et Transmission* **2**, 61–74 (1948).
- [106] A. Einstein, *Sitz. Ber. Preuss. Akad. Wiss.* **23** pp. 18 – 25 (1925).
- [107] J.D. Franson, *Phys. Rev. Lett.* **62**, 2205–2208 (1989).
- [108] J. Brendel, N. Gisin, W. Tittel, and H. Zbinden, *Phys. Rev. Lett.* **82**, 2594 (1999).
- [109] I. Marcikic, H. de Riedmatten, W. Tittel, V. Scarini, H. Zbinden, and N. Gisin, *Phys. Rev. A* **66**, 062308 (2002).
- [110] J. Splettstoesser, M. Moskalets, and M. Büttiker, *Phys. Rev. Lett.* **103**, 076804 (2009).
- [111] R. Ionicioiu, G. Amaratunga, and F. Udrea, *Int. J. Mod. Phys. B* **15**, 125 (2001).
- [112] P. Samuelsson and M. Büttiker, *Phys. Rev. B* **73**, 041305R (2006).
- [113] M. Nielsen and I. Chuang, *Quantum computation and quantum information* (Cambridge University Press, 2000).
- [114] S. Hill and W.K. Wootters, *Phys. Rev. Lett.* **78**, 5022–5025 (1997).
- [115] W.K. Wootters, *Phys. Rev. Lett.* **80**, 2245–2248 (1998).
- [116] C.H. Bennett, D.P. DiVincenzo, J.A. Smolin, and W.K. Wootters, *Phys. Rev. A* **54**, 3824–3851 (1996).
- [117] W. Wootters, *Quantum Information and Computation* **1**, 27 (2001).
- [118] M. Moskalets and M. Büttiker, *Phys. Rev. B* **66**, 205320 (2002).
- [119] M. Devoret, *Quantum circuits and signals (part I)*, Lectures at Collège de France, 2008.
- [120] M. Moskalets, *Phys. Rev. B* **91**, 195431 (2015).
- [121] R. Landauer, *Nature* **392**, 658 (1998).
- [122] P. Hofer, D. Dasenbrook, and C. Flindt, *On-demand entanglement generation using dynamic single electron sources*, To appear in the present volume: DOI:10.1002/pssb.201600582 (2016).
- [123] K.H. Thomas and C. Flindt, *Phys. Rev. B* **91**, 125406 (2015).
- [124] D. Dasenbrook, J. Bowles, J.B. Brask, P.P. Hofer, C. Flindt, and N. Brunner, *New Journal of Physics* **18**, 043036 (2016).
- [125] N.M. Chtchelkatchev, G. Blatter, G.B. Lesovik, and T. Martin, *Phys. Rev. B* **66**, 161320 (2002).
- [126] P. Samuelsson, E. V. Sukhorukov, and M. Büttiker, *Phys. Rev. Lett.* **91**, 157002 (2003).
- [127] P. Samuelsson and M. Büttiker, *Phys. Rev. B* **71**, 245317 (2005).
- [128] V. Giovannetti, D. Frustaglia, F. Taddei, and R. Fazio, *Phys. Rev. B* **74**(11), 115315 (2006).
- [129] V. Giovannetti, D. Frustaglia, F. Taddei, and R. Fazio, *Phys. Rev. B* **75**, 241305 (2007).
- [130] Y. Sherkunov, N. d’Ambrumenil, P. Samuelsson, and M. Büttiker, *Phys. Rev. B* **85**, 081108 (2012).